PNAS

Main Manuscript for

The role of astrocytes in depression, its prevention and treatment by targeting astroglial gliotransmitter release

Yorley Duarte[1†], Daisy Quintana-Donoso[2†], Rodrigo Moraga-Amaro[2], Ivanka Dinamarca[2], Yordan Lemunao[2], Kevin Cárdenas[2], Tamara Bahamonde[2], Tabita Barrientos[2], Pedro Olivares[1], Camila Navas[1], Francisco J. Carvajal[3], Yessenia Santibánez[2], Raimundo Castro-Lazo[2], María Paz Meza[2], Ramon Jorquera[4], Gonzalo I. Gómez[5], Marina Henke[6], Rodrigo Alarcón[7], Laureen A. Gabriel[6], Susanne Schiffmann[6], Waldo Cerpa[3], Mauricio A. Retamal[7], Felipe Simon[8-10], Sergio Linsambarth[2], Fernando Gonzalez-Nilo[1,11] and Jimmy Stehberg[1,2*]

[1]Center for Bioinformatics and Integrative Biology, Facultad de Ciencias de la Vida, Universidad Andres Bello, Santiago 8370146, Chile

[2]Laboratorio de Neurobiología, Instituto de Ciencias Biomédicas, Facultad de Medicina. Universidad Andres Bello, Santiago, Chile.

[3]Laboratorio de Función y Patología Neuronal, Departamento de Biología Celular y Molecular, Facultad de Ciencias Biológicas, Pontificia Universidad Católica de Chile, Santiago, Chile.

[4]Instituto de Ciencias Biomédicas, Facultad de Medicina. Universidad Andres Bello, Santiago, Chile.

[5]Laboratorio de Fisiología Renal y Comunicación Celular, Instituto de Ciencias Biomédicas, Facultad de Ciencias de la Salud, Universidad Autónoma de Chile, Santiago 8910060, Chile.

[6]Fraunhofer Institute for Molecular Biology and Applied Ecology IME, Project Group Translational Medicine and Pharmacology (TMP), Theodor-Stern-Kai 7, 60590 Frankfurt/Main, Germany

[7]Programa de Comunicación Celular en Cáncer, Universidad del Desarrollo, Facultad de Medicina Clínica Alemana, Santiago, Chile.

[8]Universidad del Desarrollo, Centro de Fisiología Celular e Integrativa. Facultad de Medicina Clínica Alemana. Santiago, Chile.

[9]Laboratory of Integrative Physiopathology, Faculty of Life Sciences, Universidad Andres Bello, Santiago, Chile.

[10]Millennium Institute on Immunology and Immunotherapy, Santiago, Chile.

[11]Millennium Nucleus of Ion Channel-Associated Diseases, Santiago, Chile.

‡ These authors contributed equally to this work

*Corresponding author.

Email: Jimmy Stehberg (jstehberg@unab.cl).

Author Contributions: YD and CN contributed with the in-silico studies; RM-A, DQ-D, YL, YS, TB & SL contributed with the in-vivo pharmacology and behavioral tests; IJ-D, MPM & GG contributed with studies in astroglial cell lines and hippocampal slices, and visualization; YL, RC-L & GG contributed with ex-vivo studies in hippocampal slices; FS & PO contributed with the in-vitro studies in HeLa and astroglial cell lines; WC & FJC contributed with slice electrophysiological recordings, SS, MH & LAG contributed with the plasmon-resonance studies; MR and RA contributed with gap junctional studies; RJ contributed with data analysis; JS, FS, & FG-N contributed with the experimental design, coordination, and supervision. JS wrote the Manuscript and designed the study.

Competing Interest Statement: MAR, DG-N & JS authored a Patent application filed in 2013-05-31 (WO 2013/179264), which was granted in the US (US-9879058-B2) on the date 2018/01/30, entitled “Use of compounds that selectively modulate astrocytic release of substances through hemichannels of connexins and pannexins, without influencing gap junctions, for the treatment of psychiatric disorders”, which included cacotheline as an example. All other authors report no conflicts of interest.

Classification: BIOLOGICAL SCIENCES, Neuroscience.

Keywords: depression, Cx43 hemichannels, TAT-Cx43L2, cacotheline, gliotransmission, astrocytes.

This PDF file includes:

Main Text
Figures 1 to 5
Table 1

Abstract

The role of ventral hippocampus (vHipp) astroglial gliotransmission in depression was studied using chronic restraint stress (CRS) and chronic unpredictable mild stress (CUMS) rodent models. CRS increased Cx43 hemichannel activity and extracellular glutamate levels in the vHipp and blocking astroglial Cx43 hemichannel-dependent gliotransmission during CRS prevented the development of depression and glutamate buildup. Moreover, the acute blockade of Cx43 hemichannels induced antidepressant effects in rats previously subjected to CRS or CUMS. This antidepressant effect was prevented by co-injection of glutamate and D-serine. Furthermore, Cx43 hemichannel blockade decreased postsynaptic NMDAR currents in vHipp slices in a glutamate and D-serine-dependent manner. Notably, chronic microinfusion of glutamate and D-serine, L-serine, or the NMDAR agonist NMDA, into the vHipp induced depressive-like symptoms in non-stressed rats. We also identified a small molecule, cacotheline, which blocks Cx43 hemichannels and its systemic administration induced rapid antidepressant effects, preventing stress-induced increases in astroglial Cx43 hemichannel activity and extracellular glutamate in the vHipp, without sedative or locomotor side effects. In conclusion, chronic stress increases Cx43 hemichannel-dependent release of glutamate and D-/L-serine from astrocytes in the vHipp, overactivating postsynaptic NMDARs and triggering depressive-like symptoms. This study highlights the critical role of astroglial gliotransmitter release in chronic stress-induced depression and suggests it can be used as a target for the prevention and treatment of depression.

Words: 214

Significance Statement

Our study demonstrates that depression, as modeled by chronic restraint stress and chronic unpredictable mild stress in rodents, is driven by increased astroglial release of glutamate and D/L-serine through Cx43 hemichannels in the ventral hippocampus. This release overactivates postsynaptic NMDA receptors (NMDARs), leading to depressive-like behaviors. These findings highlight the critical role of astroglial gliotransmitter release in the pathogenesis of depression and suggest that targeting astrocytes can both prevent and treat depression. We also identify a novel small molecule inhibitor of Cx43 hemichannels with antidepressant properties. Our study makes novel and

important contributions to the understanding of the mechanisms by which aberrant glutamatergic activity in the ventral hippocampus occurs and contributes to depression.

Introduction

In depression, available antidepressants target neuronal neurotransmitter-related mechanisms including neurotransmitter uptake (SSRIs, TCAs), degradation (MAOIs) or their post-synaptic receptors (vortioxetine, ketamine). However, neurons are not the only brain cells that participate in synapses. Astrocytes are the most abundant glial cells in the brain and release their own transmitters, dubbed gliotransmitters (for a review, see (1)) onto glutamatergic and GABAergic synapses. In Major Depression (MD), astrocytes suffer a reduction in their cell density in brain regions relevant to depression, based on clinical (2, 3), post-mortem (2) and rodent (4, 5) studies, suggesting that their dysfunction may be associated to the pathogenesis of depression.

One of the key brain regions associated with depression and among the most studied is the ventral hippocampus (reviewed in (6)), in which depression is associated with increased extracellular glutamate in MD patients (7), and in animal models for depression (8–10).

Astrocytes are critical for the regulation of synaptic glutamate via both recycling synaptic glutamate and releasing glutamate onto synapses, directly affecting glutamatergic synaptic transmission (reviewed in [11]). In both MD patients and animal models for depression, evidence suggests that astrocytes in the hippocampus have a reduced expression of glutamate transporters, suggesting decreased synaptic clearance of glutamate (8, 11), which contributes to the increased extracellular glutamate.

We have previously reported that chronic restraint stress (CRS)-one of the main rodent models for depression-, induces a large increase in astroglial Cx43 hemichannel activity in the ventral hippocampus, associated to a large Cx43 hemichannel-dependent increase in extracellular glutamate and ATP (12). Cx43 hemichannels are one of the main pathways for the astroglial release of gliotransmitters like glutamate and ATP (13–15) and have been shown to be the main pathway of astroglial release of glutamate and ATP in the hippocampus in response to GABA (16).

The idea that astroglial Cx43 hemichannel-dependent gliotransmission is associated with depression is supported by several studies. One study showed that chronic corticosterone-induced depression is associated with increased astroglial Cx43 phosphorylation (17), known to increase hemichannel activity and decrease gap junctional activity (18). Antidepressant treatment normalized Cx43 phosphorylation (17), whilst exposure to antidepressants reduced astroglial Cx43 hemichannel activity in astroglial primary cultures (19). Direct evidence of a causal role for increased gliotransmission in the pathophysiology of MD is still lacking. However, a recent study reported that the oral administration of a novel Cx43 hemichannel blocker dubbed D4, showed antidepressant effects when administered after the end of stress in the CRS rodent model of depression. The treated animals showed reduced anxiety- and depression-like behaviors including learned helplessness and anhedonia (20). Hence, there is increasing evidence that astroglial gliotransmission via Cx43 hemichannels may contribute to depression, but the mechanisms that subserve such a contribution have not been studied to date. In the present study, we evaluated the role of gliotransmission and specifically, astroglial Cx43 hemichannel-dependent gliotransmission, in the development of depressive-like behavior in the rat models of CRS and unpredictable mild stress (CUMS), and whether they could be targeted for the development of antidepressants. Given that the previous study using CRS showed antidepressant effects of Cx43 blockade in both learned helplessness and anhedonia (20), only learned helplessness was used here as a surrogate for depressive-like behaviors.

One of the benefits of studying Cx43 hemichannels is that in the brain, Cx43 is only expressed in astrocytes (21, 22), so it is possible to selectively interfere with their activity, affecting astroglial gliotransmission. The pharmacological blockade of Cx43 hemichannels is attained by a mimetic peptide known as TAT-Cx43L2 (henceforth, TAT-L2), which is cell permeable and selectively decreases Cx43 hemichannel activity without directly affecting inter-neuronal (synaptic) or gap junction-mediated inter-astroglial communication (13, 22). The TAT-L2 peptide has been widely used to identify Cx43 hemichannel-dependent astroglial tracer uptake and gliotransmission (12, 16, 22, 23).

Results

To evaluate the involvement of ventral hippocampal astroglial Cx43 hemichannels in depression, TAT-L2 was chronically microinjected into the ventral hippocampus using osmotic pumps throughout the 10 days of CRS, which was employed to induce depressive-like behaviors in rats (see experimental design in **Fig. 1A**). As shown in **Figure 1B**, CRS (veh, black) induced depressive-like symptoms, increasing immobility in the tail suspension test (TST), compared to non-stressed animals (**Fig. 1B**, veh, white). Notably, the chronic blockade of Cx43 hemichannels with 10 nM TAT-L2 during CRS (**Fig. 1B**, TAT-L2) prevented the development of depressive-like symptoms.

In a recent study, we reported that in the basolateral amygdala (BLA), the acute microinjection of TAT-L2 blocked both short-term and long-term fear memory, but not learning. This effect was prevented by the addition of glutamatergic NMDA receptor (NMDAR) co-agonists glutamate and D-serine together, but not by each individually. TAT-L2 also reduced postsynaptic NMDAR activity in BLA slices, an effect similarly prevented by a mixture of glutamate and D-serine, but not by each alone (23). Astroglial Cx43 hemichannels were also shown to regulate postsynaptic NMDAR activity in the prefrontal cortex via D-serine (24). Given that CRS increases astroglial Cx43 hemichannel activity and the Cx43 hemichannel-dependent release of glutamate (12), and since Cx43 hemichannels regulate postsynaptic NMDAR activity via the release of its co-agonists glutamate and D-serine (24), and given the critical role of NMDARs in depression and in the antidepressant effects of the NMDAR antagonist ketamine (25), we decided to test whether the chronic microinfusion of glutamate and D-serine could prevent the effects of TAT-L2. Consequently, TAT-L2 was co-injected with a combination of glutamate and D-serine, which recovered the development of depressive-like behaviors, despite the blockade of Cx43 hemichannels (**Fig. 1B**, TAT-L2 + glutamate + D-serine, black). The co-injection of TAT-L2 with either glutamate or D-serine individually did not prevent the effects of TAT-L2 (see **Supplementary Fig. S1A**).

If depressive-like symptoms are induced by chronic stress via the increased release of a combination of glutamate and D-serine, then one would expect that the chronic microinfusion of both glutamate and D-serine into the ventral hippocampus,

should be sufficient to induce depressive-like symptoms in non-stressed rats. This was indeed observed (**Fig. 1B**, glutamate + D-serine, white). To further understand whether depressive symptoms are induced by the combination of glutamate and D-serine, or by each separately, either glutamate, D-serine or their combination was microinfused chronically into the ventral hippocampus for 10 days without stress. Unexpectedly, not only the combination of glutamate and D-serine (**Fig. 1C**, glutamate + D-serine, white) but also D-serine alone (**Fig. 1C**, D-serine, white), induced depressive-like symptoms, while glutamate alone (**Fig. 1C**, glutamate, white) did not.

Studies have shown that astrocytes are a significant source of brain D-serine, expressing the enzyme serine racemase that converts L-serine into D-serine (26). However, neurons can also covert L-serine and release D-serine (27). Given that astrocytes mediate the transport of amino acids and glucose across the brain blood barrier and express the enzyme that converts glucose into L-serine (28), it is possible that Cx43 hemichannels mediate the astroglial release of L-serine, which could then be converted into D-serine by neurons expressing serine racemase. To assess this possibility, we repeated the previous experiment, chronically microinfusing either glutamate, L-serine or a mixture of glutamate and L-serine into the ventral hippocampus for 10 days. The logic was that if L-serine rather than D-serine is released by astrocytes, L-serine would be expected to have the same effect as D-serine, inducing depressive-like symptoms. Interestingly, the microinjection of L-serine was able to induce depressive-like symptoms (**Figure 1D**, L-serine, white), but the combination of glutamate and L-serine did not (**Figure 1C**, glutamate + L-serine, white). This suggests that both D- and L-serine are released by astrocytes, but the conversion of L-serine to D-serine in neurons may be regulated by glutamate. This idea is further supported by the observation that chronic D-serine alone was not sufficient to prevent the effects of Cx43 hemichannel blockade, indicating that adding glutamate is necessary when blocking Cx43 hemichannels for D-serine to counteract the effects of TAT-L2. This is consistent with previous studies suggesting that the activity of serine racemase is highly regulated and activated by glutamate through its interaction with the glutamate receptor interacting protein (29) and via AMPA receptor activation (30).

The present results support the notion that chronic stress induces an increase in Cx43 hemichannel-dependent release of glutamate and D-serine (and/or L-serine). This

suggests that the chronic increase in hippocampal D-serine/L-serine is sufficient to induce depressive-like symptoms in the presence of normal glutamate levels but is insufficient to rescue depressive symptoms when Cx43 hemichannels are blocked, requiring the exogenous addition of glutamate.

In conclusion, the astroglial release of glutamate and D-serine (and/or L-serine) is involved in the physiopathology of CRS-induced depression in rats. Henceforth, we continued the experiments with D-serine, but it is likely that both D- and L-serine show similar effects.

Taken together, the present evidence suggests that the Cx43 hemichannel-dependent release of glutamate and D-serine (whether released directly by astrocytes, produced via conversion of L-serine by neighboring neurons) could act on post-synaptic NMDARs, inducing an overactivation of hippocampal NMDARs, which has been reported in depressed patients and animal models of depression (31, 32). If this were to be true, the pharmacological overactivation of postsynaptic NMDARs in the ventral hippocampus should induce depressive like-symptoms in the absence of stress. To test this, we microinfused the NMDAR agonist NMDA into the ventral hippocampus for 10 days without stress and found that the chronic activation of NMDARs with NMDA resulted in depressive-like symptoms in non-stressed animals (**Figure 1E**, NMDA).

The osmotic pumps that were used in the present experiments released the loaded compounds continuously into the ventral hippocampus for 14 days. Since they were implanted 4 days before beginning the chronic stress protocol, the depressive-like symptoms were measured on day 14 after pump implantation, the last day of drug delivery. It may be argued that while TAT-L2 is being released, there may be antidepressant effects that recede once the peptide is not being delivered, suggesting TAT-L2 induces antidepressant effects rather than preventing depression. To assess this possibility, vehicle, TAT-L2 or TAT-L2 + glutamate and D-serine were microinfused during the 10 days of chronic stress, but the animals were tested for depressive-like symptoms (TST) on day 18, 4 days after drug release ended. As shown in **Figure 1F**, TAT-L2 prevented the development of depressive-like symptoms, as evidenced by no depressive-like symptoms 4 days after the end of TAT-L2 administration, while animals

263 microinfused with TAT-L2 + glutamate + D-serine still showed depressive-like
264 symptoms.

265 We then evaluated whether blocking Cx43 hemichannels could induce
266 antidepressant effects in animals that had already undergone CRS. TAT-L2 was
267 microinjected into the ventral hippocampus acutely, using chronically implanted
268 cannulas, after the 10 days of CRS (see **Fig. 2A** for the experimental design). As shown
269 in **Figure 2B**, the acute pharmacological blockade of Cx43 hemichannels induced
270 antidepressant effects in rats that had undergone CRS, evidenced by increased
271 immobility (**Fig. 2B**, TAT-L2) and decreased struggle (**Supplementary Figure S1B**) in
272 the TST, an effect prevented by co-injection with glutamate and D-serine (**Fig. 2B**, TAT-
273 L2 + glut + D-serine; **Supplementary Fig. S1B**, TAT-L2 + glut + D-serine). Notably, the
274 acute administration of glutamate and D-serine into the hippocampus induced
275 depressive-like symptoms in non-stressed animals (**Fig. 2B**, Glut + D-serine)**.**

276 We then tested whether the combination of glutamate and L-serine could prevent
277 the antidepressant effects of TAT-L2 and found that co-injection of TAT-L2 with
278 glutamate and L-serine also abolished the antidepressant effects of TAT-L2 in animals
279 that had undergone CRS (**Fig. 2C**, TAT-L2 + glut + L-serine). The co-injection of TAT-L2
280 with glutamate, D-serine or L-serine individually did not prevent the effects of TAT-L2
281 (see **Supplementary Fig. S1C**). Additionally, TAT-L2 had no effects on immobility when
282 microinjected into the ventral hippocampus of control non-stressed rats (**Supplementary**
283 **Fig. S1D**).

284 To ensure that the antidepressant effects of Cx43 hemichannel blockade were
285 not dependent on the test used to measure depressive-like symptoms, the previous
286 experiment with CRS was repeated, now using the forced swim test (FST). As shown in
287 **Figures 2D** and **2E**, TAT-L2 induced antidepressant effects as measured in the FST, an
288 effect again prevented by the co-injection of TAT-L2 with a combination of glutamate and
289 D-serine (**Fig. 2D**, TAT-L2 + glutamate + D-serine) and with glutamate and L-serine
290 (**Fig. 2E**, TAT-L2 + glutamate + L-serine). Similarly to what was observed with the TST,
291 the co-injection of TAT-L2 with either D-serine or L-serine prevented the effects of TAT-
292 L2, but not glutamate alone (see **Supplementary Fig. S1E**).

To confirm that the antidepressant effects obtained by Cx43 hemichannel blockade and their prevention with glutamate and D-serine are general principles applicable to other rodent depression models, TAT-L2 was microinjected into the ventral hippocampus after CUMS, alone or together with glutamate and D-serine. As shown in **Figure 2F**, CUMS induced a significant increase in immobility in the TST, consistent with depressive-like behavior, which was significantly reduced by intra-hippocampal TAT-L2, an effect again prevented by co-injection with glutamate and D-serine (**Figure 2F).**

To corroborate that chronic stress induces an increase in astroglial Cx43 hemichannel activity, Etd+ uptake was measured in rat hippocampal slices the day after 10 days of CRS, and the incubation media was analyzed for extracellular glutamate. As shown in **Figure 2G**-**H**, CRS (Veh, black bar) induced a large increase in Etd^{+} uptake in GFAP-labelled astrocytes compared to controls (without stress, Veh, white bar). This effect was also observed when analyzing the percentage of GFAP+/Etd+ cells (**Supplementary Fig. S1F**). The percentage of GFAP+ cells showing Etd+ uptake increased from 11.93% ± 0.99 (non-stressed) to 31.00% ± 2.08 (stressed, $p<0.001$). This increase was prevented by preincubation with TAT-L2, which decreased uptake to 10.00% ± 0.58 ($p<0.001$). These results indicate that CRS increases both Etd+ uptake per astrocyte and the percentage of astrocytes showing uptake. Preincubation with TAT-L2 prevented these increases, demonstrating that the uptake was mediated by Cx43 hemichannels.

As can be seen in the **Supplementary Table 1**, in the case of non GFAP-labeled cells, which could potentially include non $GFAP^{+}$ astrocytes, neurons, microglia, oligodendrocytes and mast cells, basal uptake under no stress was observed in 17%± 2.39% of the cells, which was increased to 36%± 2.31% after CRS. However, uptake in non GFAP-labeled cells was unaffected by Cx43 hemichannel blockade with TAT-L2, rendering 31.33%± 1.86% of the non-GFAP labeled cells with uptake. This is consistent with the lack of Cx43 hemichannels in other brain cells under physiological conditions and suggests that the uptake was not mediated by Cx43 hemichannels, ruling out non-$GFAP^{+}$ astrocytes. In conclusion, the number of astrocytes (GFAP-labeled cells) that showed increased Cx43 hemichannel activity tripled after CRS, while other non-Cx43 expressing cell types (likely neurons) also showed an increase in uptake, which was not mediated by Cx43 hemichannels, as it was unaffected by TAT-L2, likely mediated by

Cx36 hemichannels, panx1 pannexons or other large pore channels expressed in other brain cell types. Analysis of the culture media from hippocampal slices after CRS showed a significant increase in extracellular glutamate (**Fig. 2I**, Veh, black bar), which was prevented by preincubation with TAT-L2 (**Fig. 2I,** TAT-L2, black bar).

The next step we took was to corroborate that TAT-L2 reduced postsynaptic NMDAR activity in the ventral hippocampus by decreasing glutamate and D-serine, as described previously for the BLA (23). Consequently, rat ventral hippocampal slices were incubated with TAT-L2, and NMDAR activity was analyzed by electrophysiological recordings in conditions that enhanced NMDAR-dependent currents, including blocking GABAergic activity, AMPARs and no Mg^{2+}. Incubation with TAT-L2 induced a decrease in NMDAR-mediated postsynaptic field potentials (fEPSP; see **Fig. 3A** for fEPSP traces and **Fig. 3B for** fEPSP amplitude), which was prevented by the addition of a combination of glutamate and D-serine. Notably, unlike BLA slices where the addition of glutamate and D-serine alone had minimal effects on TAT-L2-induced reduction in NMDAR activity (23), in the ventral hippocampus, both had a more pronounced effect when added individually (**Supplementary Fig. S2A-B)**, suggesting that the hippocampus may be less dependent on astroglial glutamate and D-serine than the BLA. The fEPSP response amplitude was completely blocked by NMDAR antagonist APV, demonstrating that NMDAR activity was being recorded (**Supplementary Fig. S2A-B)**.

Previous studies have shown that TAT-L2 does not directly affect neuronal synapses as measured by glutamate and ATP release from neuronal primary cultures, gap junction-mediated inter-astrocyte communication (13, 22) or NMDAR activity in primary neuronal cultures without astrocytes (23). However, to further demonstrate that the effect of the TAT-L2 peptide is mediated by the blockade of astroglial Cx43 hemichannels and not by a direct effect on NMDARs, mature hippocampal primary cultures were incubated with TAT-L2 in the presence or absence of NMDAR agonist NMDA. As shown in **Figure 3C-D**, TAT-L2 had no effect on NMDAR activity or on NMDAR responses to NMDA as assessed by the Fluo-3/Fura Red fluorescence ratio in primary hippocampal neurons devoid of astrocytes, ruling out direct effects of the peptide on NMDARs and suggesting that the presence of astrocytes is necessary for the TAT-L2 to affect NMDAR activity.

If blockade of Cx43 hemichannels in the hippocampus induces antidepressant effects, targeting astroglial Cx43 hemichannels could be a potential strategy for developing antidepressants. However, TAT-L2, being a peptide, has a short half-life and is not optimal for clinical applications. Therefore, we set out to identify small molecules that could block Cx43 hemichannel activity and potentially have antidepressant effects when administered systemically. Hence, we analyzed the region of the Cx43 C-terminal domain that could putatively comprise the binding site of the TAT-L2 peptide to Cx43. Previous studies using site mutations (33) have suggested that TAT-L2 (in its shorter version, GAP19) binds to the C-terminal (CT) of Cx43, which is involved in the hemichannel closure at a low pH (34) resembling the "ball-and-chain" gating mechanism proposed for voltage-gated sodium channels (35). To confirm binding between the Cx43 CT and the TAT-L2 peptide, a surface plasmon resonance assay was performed between a synthetic Cx43 CT and the TAT-L2 peptide. We found a strong interaction between TAT-L2 and the CT (**see Supplementary Fig. S2C**), with a binding KD of 1.28 ± 0.06 µM. Hence, molecular docking was performed between the crystalized structure of the Cx43 CT (PDB id: 1R5S) and GAP19 (amino acid sequence KQIEIKKFK), which is the minimal sequence from TAT-L2 lacking the TAT motif, capable of blocking Cx43 hemichannels without affecting Cx43 gap junctional communication (13). The interaction between GAP19 and the CT was modeled via molecular dynamics simulations.

To determine the most probable binding site of GAP19 to the CT, three exploratory docking simulations were performed using different grid sizes with the AutoDockVina program (36). The grid that showed the most favorable binding energy for Gap19/CT complex formation (-5.9 kcal/mol) was selected. Then, a molecular dynamics simulation was performed for the peptide/CT complex to obtain a more stable CT structure. Analysis of the binding site and chemical properties of the CT revealed that the putative interaction between GAP19 and the CT domain was mainly electrostatic (**Fig. 3E**). At the end of the simulation, the electrostatic component became more negative, giving a stable conformation for the peptide/CT complex (**Fig. 3F**). This suggests that the four positive and one negative charges of lysine and glutamic acid of the peptide could be in contact with charged, polar, and hydrophobic residues of the Cx43 CT domain. All relevant residues in the CT were stable during the simulation. The amino acids of the CT domain that make up the putative binding site correspond to

K258, N269, Q304, A305, S306, E307, Q308, W310, D339, N341, A344, K345, A348, H351, E352, Q354, I358, V359, D360, which would share hydrogen bonds with residues of GAP19, as shown in **Fig. 3F**.

Based on these amino acids, a region of interest (grid) was set within the CT domain sequence, which included the amino acids putatively required for the interaction, and a structure-based virtual screening using the ZINC database (37, 38) was performed. This involved analyzing the possible binding of 2,063,314 compounds obtained from diverse small molecule libraries to the region of interest within the Cx43 CT. Two criteria were applied sequentially to filter the resulting compounds obtained by AutoDockVina. First, the 1,000 top-ranked compounds with the highest theoretical binding energy (lowest binding core) for the Cx43 CT domain were selected. Then, two different drug-likeness criteria were applied to exclude unsuitable compounds: logP (pH = 7.0) $\leq$ 5.0 (to increase their probability of crossing the blood-brain barrier and cell membranes) and low free energy, calculated based on predicted ADMET properties obtained using the Qikprop program. Finally, the violation number of Lipinski's rule of five (39) was used as a final filter to obtain small molecules that met drug-like criteria. All the compounds that did not meet any of the above criteria were removed from the final list, and the remaining candidates were used to run a final molecular docking against the Cx43 CT.

Several of the candidate compounds were obtained and tested *in vitro* using DAPI uptake in HeLa cells transfected with the Cx43 gene to assess their Cx43 hemichannel blocking effects, and in HeLa cells transfected with the Cx30 gene, the second most expressed Cx in astrocytes (40), to assess their specificity. The screening assay was conducted with three different concentrations (0.1µM, 10µM, and 100 µM) of each compound, using TAT-L2 as control to ensure that the tracer uptake was exclusively via Cx43 hemichannels. Among the screened compounds, cacotheline (ZINC26730911; 2,3-Dihydro-4-nitro-2,3-dixo-9,10-secostrychnidin-10-oic acid) demonstrated a similar pattern of potentially forming two hydrogen bonds with the residues Q308 and N312 of the Cx43 CT domain, and a strong electrostatic interaction with E307, confirming the accurate selection of the putative binding site (**Fig. 4A**). This interaction was empirically corroborated by surface plasmon resonance analysis with an immobilized synthetic Cx43 CT, showing that cacotheline binds to the CT with a KD of

44 ± 14 µM (**Supplementary Fig. S2D**). Cacotheline shows a theoretical affinity for the Cx43 CT domain of -8.3, and a LogP of -2.88**.**

To evaluate the effects of the compounds on Cx hemichannel activity, tracer uptake assays were employed. Tracers like DAPI or Etd^{+} can only enter living cells through non-selective large pore channels like Cx hemichannels. Cacotheline did not affect Cx43 hemichannel activity under normal calcium conditions, where hemichannels have a low open probability, suggesting that cacotheline does not induce hemichannel opening (see **Fig. 4B** for 0.1 µM and **Supplementary Fig. S3A** for 1 µM). However, cacotheline completely blocked hemichannel-mediated uptake in HeLa cells transfected with Cx43 when incubated in a bivalent cation (calcium)-free medium, which increases hemichannel activity (41), preventing dye uptake, while having no effects on Cx30 hemichannels **(Fig. 4C).** For 1 µM of cacotheline see **Figure S3B**. The IC50 of cacotheline was estimated at 0.488 ± 0.027 µM in Cx43 expressing HeLa cells (**Fig. 4D**).

To determine the effects of cacotheline on the target cells —astrocytes—, a rodent astroglial cell line (DI TNC1) known to express connexin 43 (42) and release glutamate through Cx43 hemichannels (16) was used. Astrocytes were incubated with DAPI (10 µM) after incubation with 0.1 µM and 1 µM cacotheline, either in the absence or presence of calcium in the medium. As with transfected HeLa cells, astrocytes showed with very little uptake under normal calcium conditions, and neither TAT-L2 nor cacotheline had any effects on uptake (**Fig. 4E**). However, astrocytes showed a large increase in dye uptake when incubated in calcium-free conditions and both 10nM TAT-L2 and 0.1µM cacotheline prevented uptake, demonstrating that they induced similar blocking effects on Cx43 hemichannels (**Fig. 4F**). Cacotheline at 1 µM also had no effects on DAPI uptake when cells were incubated in normal calcium (**Supplementary Fig. S3C)**, but blunted dye uptake in astroglia incubated in calcium-free conditions (**Supplementary Fig. S3D**). A dose-response curve showed that cacotheline had an IC50 of 59.62 ± 6.42 nM in DI NCT1 astrocytes (**Fig. 4G**). The blocking effects of cacotheline on Cx43 hemichannels were corroborated directly on Cx43 hemichannel conductance by patch clamp electrophysiological recordings of single Cx43 transfected HeLa cells (**Supplementary Fig. S3E**).

Cacotheline is an alkaloid nitro derivative of brucine, from the strychnine family (t. E. Merck Index, 1604), previously used as a redox indicator in titrations that involve tin ions (Sn^{2+}) (43). However, no biological activity has been previously reported. It contains an indole ring, one carboxylic acid, and donor/acceptor groups such as the N group, potentially involved in binding to the Cx43 CT. Considering its alkaloidal nature, a cell viability assay (3-(4,5-Dimethylthiazol-2-yl)-2,5-Diphenyltetrazolium Bromide, MTT) was performed at different concentrations, from 0.1 µM to 100 mM at variable times (0 to 96 hours). Cacotheline showed low cellular toxicity at concentrations under 0.5 mM (**Supplementary Fig. S3F**). Neither cacotheline nor, -as previously reported TAT-L2 (*19*), effected gap junction-mediated inter-astrocyte communication, as measured by the scrap & load technique in rat primary cortical astrocytes (**Supplementary Fig. S4A**).

To ensure that the effects of TAT-L2 were not specific to the ventral hippocampus, dorsal hippocampal slices were incubated with 50 nM TAT-L2 with or without glutamate (10 µM) and D-serine (10 µM), and post synaptic NMDAR activity was recorded. As with the ventral hippocampus, TAT-L2 induced a decrease in evoked NMDAR activity which was prevented by glutamate and D-serine (**Supplementary Figure S4**), as can be observed in slopes of input/output curves (**Supplementary Figure S4B**). Interestingly, when hippocampal slices were incubated with two different concentrations of TAT-L2 (30 nM and 50 nM) and stimulated with increased stimulus intensity, the reductions in fEPSPs, though were greater with higher TAT-L2 dosage, reached an asymptote around 40% (see **Supplementary Figure S2C** for fEPSP single traces and **Figure S2D** for slopes of input/output curves). This suggests that TAT-L2 decreases NMDAR activity, but it is likely unable to completely block it.

To confirm that cacotheline has the same effects on NMDAR-mediated activity as the TAT-L2 peptide, dorsal hippocampal slices were incubated with 1 µM cacotheline with or without glutamate (10 µM) and D-serine (10 µM), using a similar preparation as for testing TAT-L2. Cacotheline (**Figure 5A**) induced a decrease in NMDAR-mediated postsynaptic fEPSPs that was very similar to the one found after TAT-L2 incubation in both ventral and dorsal hippocampi. This effect was also partially prevented by the addition of glutamate and D-serine and abolished by their combination, as can be observed in single traces (**Fig. 5A,** left) and fEPSP slopes of input/output curves (**Fig. 5A**, right).

To evaluate the potential antidepressant effects of cacotheline, rats subjected to 10 days of CRS were administered cacotheline intraperitoneally at 120 mg/kg one day after CRS and tested 30 minutes later in both the TST and FST. Cacotheline induced significant antidepressant effects, reflected by a reduction in immobility time in both the FST (**Fig. 5B**) and the TST (**Fig. 5C**). The antidepressant effect was comparable to that of a sub-sedative dose of intraperitoneal ketamine (**Fig. 5D**) and to 21 days of oral fluoxetine (**Fig. 5E**). To exclude the possibility that cacotheline could be inducing sedative effects or affect locomotion, injected animals were tested in an open field, which revealed a non-significant tendency for increased locomotion (**Fig. 5F**), ruling out possible sedative effects.

To confirm that the antidepressant effects induced by cacotheline were mediated by blocking chronic stress-induced increases in astroglial Cx43 hemichannel activity and glutamate release in the ventral hippocampus, Cx43 hemichannel activity was measured using Etd^{+} uptake in rat hippocampal slices from animals subjected to CRS for 10 days and administered 120 mg/kg cacotheline i.p. the next day. CRS induced a significant increase in Etd+ uptake in hippocampal GFAP-labeled astrocytes (Veh, black) compared to control animals (Veh, white bar), which was completely blunted by cacotheline administration (**Fig. 5G-H**). This effect was similar to that obtained with TAT-L2 preincubation in slices from stressed animals (TAT-L2, black bar), indicating that cacotheline prevents CRS-induced increases in astroglial Cx43 hemichannel activity. Furthermore, analysis of the culture medium of the hippocampal slices showed that CRS induced a significant increase in extracellular glutamate (**Fig. 5I**, Veh, black bar), which was prevented by cacotheline administration (**Fig. 5I,** Caco, red bar) to levels similar to TAT-L2 preincubation in slices from stressed animals. Consequently, the i.p. administration of cacotheline induces rapid antidepressant effects by decreasing astroglial Cx43 hemichannel-dependent gliotransmission, preventing extracellular glutamate accumulation, and reducing postsynaptic NMDAR activity in the hippocampus.

To determine whether the antidepressant effects of a single acute dose of 120 mg/kg cacotheline were still present 7 days afterwards, rats subjected to CRS were administered cacotheline the next day and tested on the TST on day 18, 7 days after the last stress session. As shown in **Supplementary Figure S5A**, both vehicle- and cacotheline-treated rats exhibited depressive-like behavior on day 18, suggesting that

unlike the chronic administration of TAT-L2 during chronic stress, which prevented the development of depressive-like behavior, the antidepressant effects of an acute dose of cacotheline did not last 7 days.

To evaluate general organ function after administration of 120 mg/kg cacotheline i.p., blood samples were taken from rats 24 hours after administration, and the plasma levels of organ function markers were analyzed. Acute cacotheline treatment had no effects on markers of renal function (BUN, creatinine, uric acid, calcium), hepatic function (total bilirubin, transaminases [ALT, AST, GGT], phosphatases [ALP], albumin and total serum proteins), and glycemia (see **Supplementary Fig. S5B-E**). To assess potential long-term toxicity, cacotheline was administered via an osmotic pump implanted subcutaneously for 28 days, continuously releasing 22.5 µg throughout the experiment in rats previously subjected to chronic stress or non-stressed. No animal mortality occurred during the 28 days of subcutaneous administration.

All data averages, SE, statistical results, and p-values ordered by figure can be found in **Supplementary Table 1.**

Discussion

The present study demonstrates for the first time that depression induced by CRS and CUMS is caused by increased activation of astroglial Cx43 hemichannels and release of gliotransmitters, including glutamate and L/D serine. These gliotransmitters increase postsynaptic NMDAR activity, which can be prevented by hippocampal blockade of Cx43 hemichannel-mediated gliotransmission during chronic stress. Consistently, chronic intra-hippocampal administration of a combination of D-serine, glutamate and L-serine, and NMDAR agonist NMDA, induced depressive-like symptoms in non-stressed rats. These findings highlight the critical role for astroglial gliotransmission and its regulation of postsynaptic NMDARs in the pathophysiology of depression, based on two major rodent models of depression.

Additionally, we identified a small molecule, cacotheline, which blocks Cx43 hemichannels and, when administered subcutaneously, produces rapid antidepressant effects by preventing increased Cx43 hemichannel activity and glutamate buildup in the ventral hippocampus. Hence, cacotheline could serve as a starting point for the

development of novel antidepressants targeting gliotransmission. This finding aligns with previous research showing that oral administration of a novel Cx43 hemichannel blocker, D4, has anxiolytic and antidepressant effects, as assessed using the open field test, TST, FST, and SPT to measure anhedonia (20). Hence, the present study contributes to the understanding of the mechanisms by which D4 induced antidepressant effects.

The evidence presented here of a critical role for astroglial Cx43 hemichannel-mediated gliotransmission in depression is consistent with previous studies showing increased Cx43 astroglial hemichannel activity in animal models of depression (12) and in depressed patients (44), which may be reduced by antidepressants both *in vivo* (17) and *in vitro* (19). This increase in Cx43 hemichannel-mediated gliotransmission after CRS is associated with increased Cx43 hemichannel activity in ventral hippocampal astrocytes rather than an increase in Cx43 protein expression (12). Notably, a previous study reported that Cx43 phosphorylation levels correlated with depression and were reduced by antidepressant treatment (17). Future studies should determine whether this increase in Cx43 phosphorylation also occurs after CRS and CUMS, and how different Cx43 phosphorylation levels may modify Cx43 hemichannel-mediated gliotransmission.

Hippocampal Cx43 hemichannel blockade induced antidepressant effects and a reduction of hippocampal NMDAR-mediated currents, both of which were prevented by the addition of glutamate and D-serine. This suggests that the antidepressant effects of Cx43 hemichannel blockade were mediated by a reduction of postsynaptic NMDAR activity. Cx43 hemichannel blockade did not directly affect NMDARs in primary hippocampal neuronal cultures, suggesting that TAT-L2 effects are mediated by astrocytes rather than a direct effect on neuronal NMDARs. Hippocampal NMDAR activity is central in the pathophysiology of depression (45) and underpins the use of the NMDAR antagonist ketamine/esketamine at sub-sedative doses as a fast-acting antidepressant (46, 47). The fact that both TAT-L2 peptide and cacotheline, shown to block astroglial Cx43 hemichannel activity, reduce postsynaptic NMDAR activity in hippocampal slices attests to the relevance of astroglial Cx43 hemichannels in regulating NMDAR activity in postsynaptic neurons, previously shown in the BLA (23) and prefrontal cortex (24). Moreover, the finding that chronic infusion of glutamate + D-serine or the NMDAR agonist NMDA into the ventral hippocampus induce depressive-like symptoms in non-stressed animals supports a model where chronic stress increases

astroglial Cx43 hemichannel-dependent release of glutamate and D-serine (and/or L-serine) in the hippocampus, which over-activates postsynaptic NMDARs, leading to depressive-like symptoms in rats.

An intriguing result from our study pertains to the plateau in NMDAR activity reduction after a TAT-L2 incubation in hippocampal slices. TAT-L2-induced inhibition of postsynaptic NMDAR activity plateaued at a ~60% reduction irrespective of the dose of TAT-L2 applied. This can be understood through at least two alternative explanations; first, astrocytes have other gliotransmitter release mechanisms besides Cx43 hemichannels, as astroglial D-serine can be released via large vesicles (48) and exocytosis (49, 50). Thus, residual D-serine may be released through these mechanisms. Second, D-serine is also released by neurons (51, 52). The plateau obtained after TAT-L2 application is particularly relevant, as it could explain why Cx43 hemichannel blockade does not induce sedative effects or show high toxicity, as it reduces but does not completely disrupt postsynaptic NMDAR activity, unlike ketamine and other NMDAR antagonists. The partial reduction in NMDAR activity by hemichannel blockade may explain its lack of toxicity, as it may not sufficiently decrease NMDAR activity to induce ketamine-associated side effects. Furthermore, astrocytes also express NMDARs (reviewed in (53)), suggesting that ketamine could potentially affect astroglial activity and astroglial networks.

It is important to note that in the intra-hippocampal chronic administration during CRS of L-serine alone prevented the effects of TAT-L2 and induced depressive-like symptoms in non-stressed animals, effects were not obtained when L-serine was co-injected with glutamate. These results could be explained by regulation of the conversion of L-serine to D-serine in neurons by glutamate, as previous studies have reported that the activity of serine racemase is activated by glutamate through its interaction with the glutamate receptor interacting protein (29) and via AMPA receptor (AMPAR) activation (30). Interestingly, when L-serine and glutamate were microinjected into the hippocampus after chronic stress, they were able to prevent the antidepressant effects of TAT-L2 in already depressed animals. Arguably, this difference might be due to the tight regulation of L-serine conversion to D-serine by glutamate under physiological conditions, which could be lost under chronic stress conditions. A similar example can be found with the dopamine precursor L-Dopa. Administration of L-Dopa in healthy

subjects does not induce involuntary motor effects known as dyskinesias (54), which increasingly appear as the disease progresses in patients suffering from Parkinson´s Disease. This supports the idea that in physiological conditions, the production and/or release of neurotransmitters from precursors is tightly regulated, but under pathological conditions, neurotransmitter levels increase proportionally to precursor levels, possibly due to dysregulation. More research will be required to assess this possibility.

Ample evidence suggests a connection between depression, chronic stress and elevated extracellular glutamate levels in the hippocampus (12, 31). This excess in extracellular glutamate is believed to be responsible for the increased neuronal NMDAR activity found after chronic stress and in depressive patients (31, 32). However, reduced AMPAR mediated glutamatergic transmission has also been consistently reported, associated with reduced hippocampal volume (reviewed in (55)). Increased NMDAR activity is known to decrease the expression, trafficking and activity of AMPARs (56, 57). Hence, paradoxically, this heightened NMDAR activity is closely associated with decreased AMPAR-mediated glutamatergic transmission. Furthermore, astroglial Cx43 hemichannel-dependent increases in extracellular ATP have also been reported after CRS (12), and astroglial ATP has also been shown to downregulate AMPAR trafficking (58) and modulate postsynaptic NMDAR activity (59). Hence, increased ATP release from astrocytes could also contribute to the decrease in AMPAR-dependent glutamatergic transmission (reviewed in (57)). We propose that increased NMDAR and decreased AMPAR transmission may primarily stem from augmented gliotransmission.

CRS triggers an increase in Cx43 hemichannel-dependent extracellular glutamate and ATP, which can be completely blocked by TAT-L2, as seen here for glutamate and as reported previously for both (12). A similar complete reduction of extracellular glutamate was also found after Cx43 hemichannel blockade in the BLA (23). These studies are consistent with studies showing that presynaptic glutamate release is dependent on astroglial Cx43 hemichannel-dependent release of glutamate precursor glutamine (60, 61), while other reports have shown that astroglial ATP, adenosine, endocannabinoids and glutamate, also regulate presynaptic glutamate release probability and vesicle pool (62–67). Hence, presynaptic glutamate release would be expected to be reduced after astroglial gliotransmission blockade and augmented after CRS-induced increases in gliotransmission.

Another critical aspect to discuss is the potential role of chronic stress-induced increase in Cx43 hemichannel activity in hippocampal excitatory/inhibitory balance. Many studies have reported both increased glutamate levels (12, 31) and decreased GABA levels (68–70) in patients with major depression and in rodent models of depression. A recent meta-analysis found both increased glutamatergic and decreased GABAergic signaling post-mortem in many brain regions of depressed patients, including the hippocampus (71). Astrocytes can release GABA (72), but in the hippocampus, the contribution of astroglial GABA to glutamatergic inhibition has been reported as low (73). In the prefrontal cortex, astroglial GABA has been associated with the development of depressive-like behaviors in the Flinders rat model of depression (74). Additionally, astrocytes participate in GABA uptake via transporters GAD1, VGAT and GAT3, which may be reduced after chronic stress (75), and in glutamate uptake, which has been shown to be reduced in different rodent models of depression (76). Both transporters are sensitive to astroglial ATP (77, 78).

Although it was not studied here, increased extracellular ATP also contributes to the development of depressive-like symptoms in rodent models of depression (e.g. (79, 80)). Astroglial ATP is released via Cx43 hemichannels within the hippocampus (Reviewed in (1, 81)), release that is augmented after CRS (12). Astroglial ATP decreases the activity of pyramidal neurons (82) and activates the inflammasome, leading to the release of cytokines IL-1β and TNF-α, which are involved in depression-associated neuroinflammation (79, 83). Furthermore, ATP released from hippocampal astrocytes increases the activity of interneurons (82, 84) via activation of P2Y receptors (85, 86). Subsequently, ATP is converted into adenosine, which can activate A1 or A2A receptors to decrease or increase excitatory synaptic transmission (62, 87, 88). However, adenosine activation of A1 receptors in CCK-positive (82) and SST-positive interneurons (84), leads to further inhibition of pyramidal neurons, inhibition that is reduced by ketamine (89) and chronic administration of antidepressants (90, 91), resulting in AMPAR-mediated synaptic potentiation (92, 93), but see (94). In consequence, although the role of ATP was not studied in the present report, it is likely that ATP acts in concert with glutamate and D-serine and is critical for the maintenance hippocampal excitatory/inhibitory balance. The future investigation of the role of

astroglial Cx43 hemichannel-mediated ATP release and its conversion into adenosine in depression is warranted.

Based on the above evidence, increased gliotransmitter release mediated by Cx43 hemichannels is likely to have a key role in regulating excitatory/inhibitory balance in the hippocampus. However, its exact role cannot be predicted from the present data. Studies measuring other gliotransmitters released via Cx43 hemichannels during chronic stress, such as ATP and GABA, and how they may affect neuronal activity, GABA and glutamate uptake, are necessary to get a broader understanding of how excitatory/inhibitory balance is affected by increased Cx43 activity in hippocampal astrocytes under the context of depression.

Another point worth noting is that our results suggest that during chronic stress, Cx43 hemichannel-mediated gliotransmission is critical for the development of depressive symptoms. This raises the question of why other mechanisms for gliotransmitter release (e.g., exocytosis) do not compensate for Cx43 hemichannel blockade. This is significant, as Cx43 hemichannel opening is tightly controlled under physiological conditions, not only allowing the release of gliotransmitters but also inducing the influx of calcium. Given that intracellular calcium is critical for most gliotransmitter release mechanisms (reviewed in (95)), it is likely that Cx43 hemichannel opening may not only mediate gliotransmitter release but also allow extracellular calcium to enter and trigger localized release of gliotransmitters through other calcium-dependent release mechanisms (96). Thus, Cx43 hemichannel opening may be an upstream step that triggers localized gliotransmitter release from astrocytes. This could explain why the astroglial release of glutamate, ATP in response to stress (12) or GABA (16) is completely blunted by Cx43 hemichannel blockade in the hippocampus, despite the existence of other gliotransmitter release mechanisms.

As we show *in silico* and *in vitro* using surface plasmon resonance, both TAT-L2 and cacotheline bind to the C-terminal tail with high affinity. Previous studies using site-directed mutations have suggested that the Cx43-CT domain participates in an intracellular gating mechanism in hemichannels by interacting with the cytoplasmatic loop (33). Hence, by mimicking the interaction between the CT and the cytoplasmatic loop of Cx43, TAT-L2 (and probably cacotheline) may trigger the closure of the pore

from the cytoplasmatic side, allowing Cx43 gap junction channels to remain active (97) while making hemichannels resistant to activation (33, 98).

The present study demonstrates for the first time that astroglial Cx43 hemichannels are critically involved in the pathophysiology of chronic stress-induced depression. Given that increased Cx43 hemichannel activity has been reported in depressive patients, it is likely that these channels play a similar role in Major Depression. We also show that targeting astroglial Cx43 hemichannels could lead to the development of antidepressants and possibly even prevent the onset of depression. Given that NMDARs contribute to a wide range of neurological diseases (99), targeting astrocytes could not only aid in the development of antidepressants but also novel drugs to treat diseases associated with NMDAR dysfunction. In conclusion, the present study suggests that increased Cx43 hemichannel-mediated gliotransmission in the ventral hippocampus could be critical for the development of depression and a novel target for its treatment and prevention.

Materials and Methods

A detailed explanation of the methods can be found in **Supplementary materials**. All procedures involving animals were performed in accordance with NIH guidelines and with the approval of the Universidad Andrés Bello Bioethical Committee (Acta 030 – 2015). Sprague-Dawley rats (approximately 60 days old, ~250 g) were caged individually at 22°C and with a 12/12 h light/dark cycle. For acute microinjections, bilateral 21G stainless steel cannulas were implanted stereotaxically (*52*) aimed at the ventral hippocampus. After recovery, a 25G injection cannula was inserted into the guide cannula and drugs (0.5 µl) were infused bilaterally at a rate of 0.25 µl/min. For chronic microinfusions, 30G bilateral cannulas were implanted into the ventral hippocampus, connected to a subcutaneously implanted 200µl osmotic pump (0.5 µl/hr for 14 days). The following drugs were used: TAT-Cx43L2 (YGRKK RRQRRRKQIEIKKFK) at 10 nM, glutamate (100 mM) L-serine (200 nM), D-serine (200 nM), cacotheline (1 µM) and NMDA (2.71 mM). To evaluate systemic antidepressant effects, cacotheline (120 mg/kg) and ketamine (5.45 g/kg) (*50*) were administered intraperitoneally. Behavioral tests were performed 30 min after compound administration. Fluoxetine (0.7 mg/kg) was administered in 20 ml drinking water daily for 21 days. To induce depressive-like symptoms, rats underwent either CRS for 2 h per day for 10 consecutive days, or Chronic Unpredictable Mild Stress (CUMS), as previously described (100) for 28 days. Depressive-like behavior was measured using the Tail suspension test (TST) and the Forced swim test (FST), 1 or 4 days after the end of the 10 days of CRS (days 14 and 18 from implantation), or the day after 28 days of CUMS (day 29). Immobility time and time spent were analyzed. At the end of the experiments, rats were perfused intracardially, fixed with 4% PFA, brains were sectioned, and Nissl stained for cannula placement and assessment of histological lesions (tissue damage or gliosis). Rats with histological lesions were excluded from analysis. All behavioral experiments were performed blinded to the experimenter. For hippocampal slice electrophysiology recordings of post synaptic NMDARs (23), transverse slices (400 µm) were obtained from both the ventral and dorsal hippocampi. For recording, the slices were incubated with 10 µM picrotoxin (PTX) to suppress inhibitory $GABA_A$ transmission, 20 µM NBQX to block AMPAR-dependent activity, and no Mg^{2+} to unblock NMDAR currents. Recording electrodes were placed in CA1 and to evoke fEPSPs, fibers in the Stratum Radiatum

were stimulated. Recordings were filtered at 2.0-3.0 kHz and sampled at 4.0 kHz. Basal excitatory synaptic transmission was measured using an input/output curve (8 stimuli between 200-900 µA, 10s interval). TAT-Cx43L2 (50 nM) or cacotheline (1 µM), with or without glutamate (10 µM) and D-serine (10 µM), were added to the ACSF in the recording chamber. At the end of the recordings, 20µM of the NMDAR antagonist APV was used to corroborate NMDAR currents.

The potential interactions between the Cx43 C-terminal domain (PDB: 1R5S) and both GAP19 (shorter sequence of the TAT-Cx43L2) and cacotheline. molecular dynamics simulations were run (*53*), resulting in a final system size of 85.730 atoms**.** The crystal structure of the Cx43 C-terminal was used for virtual screening with the ZINC database (*23*) of commercially available compounds. Molecular docking for 2,063,314 compounds was performed. The 1,000 compounds that had the lowest binding score were filtered with two drug-likeness criteria: logP, and Lipinski's rule of five (101, 102). A total of 65 molecules were obtained and tested *in vitro* using dye uptake. Wildtype, Cx30-, Cx43-stably transfected HeLa cells and the astroglial cell line DI TNC1 grown to 80% confluence were incubated in a solution either with calcium or bivalent cation free. TAT-Cx43L2 (10 nM) and cacotheline (0.1 and 1µM) were added and then incubated with DAPI. Average fluorescence intensity per cell and percentage of DAPI labeled cells were estimated and the percentage of inhibition of fluorescence was plotted against a dose-response curve to extrapolate the IC50. Calcium imaging in hippocampal primary neuronal cell cultures was performed on C57BL6 mouse hippocampal neurons prepared from embryonic day 18 (103) and cultured over a feeder layer of glia (104). Live-cell calcium imaging was performed with the calcium-sensitive dyes Fluo-3 (5 µM) and Fura Red (15 µM) in ACSF without Mg^{2+}. D-serine (100 µM) and different concentrations of TAT-Cx43L2 (0, 10 and 100 µM) and finally, 50 µM NMDA were added with or without prior MK-801 were added. Fluo-3/Fura Red fluorescence intensity ratio in cell bodies of isolated neurons without surrounding glial cells were normalized to the mean of vehicle values. For dye uptake measurements, hippocampal slices (400 µm) were obtained from rats with or without the i.p. administration of vehicle or cacotheline (120 mg/kg), maintained with ACSF bubbled with carbogen for 60 min and then ethidium uptake "snapshot" assays were performed (12, 22). The slices were then sectioned (40µm) and immunofluorescence against astroglial GFAP was performed. Dye uptake was calculated as: corrected total cell ethidium fluorescence intensity (as arbitrary units [AU])

= integrated density – ([area of selected cell] x [mean fluorescence of background readings]). Fluorescence intensity was measured in GFAP positive cells (astrocytes) from the same quadrants that were analyzed for counting DAPI labelled cells (N=3 with triplicates). Extracellular glutamate from hippocampal slices was measured from the ACSF removed before the addition of ethidium, using a colorimetric enzyme-linked assay for indirect quantification of glutamate.

Data are expressed as Mean ± SEM. For multiple comparisons, normally distributed data were analyzed by a one-way or two-way ANOVA (as appropriate), followed by Bonferroni *post hoc* test. When comparing only 2 groups, an unpaired student's t-test was used. When data was not normally distributed, the Kruskal-Wallis test or the Wilcoxon test were used as appropriate. Differences were considered significant when $p<0.05$, and shown as $p^*<0.05$, $p^{**}<0.01$ or $p^{***}<0.001$.

Acknowledgments

We wish to acknowledge the work of the **National Cancer Institute**, which allows the use of their compound Libraries at no cost, making drug discovery available for all. We also wish to thank Maxs Méndez, Daniel Verdugo and Ivan Alfaro (Merkén) for their technical assistance and Eugenia L. Weiss for proof reading.

Funding

This work was funded by Grants FONDECYT N°1240804 (JS), N°1200452 (JS), N°1201039 (FS), N°1170733 (FG-N), N°1221498 (FG-N), N°1160227 (MR), N°11201113 (YD), CORFO INNOVA 14IDL2-30195 (JS), Proyecto Interno Universidad del Desarrollo 23.400.521 (MAR), Programa de Investigación Asociativa (PIA): Grant Anillo de Ciencia y Tecnología ACT1411, BMBF 20150065 (PCI), The Millennium Nucleus of Ion Channel-Associated Diseases (MiNICAD), supported by the Iniciativa Científica Milenio ANID (FS), PMI UAB1301 (JS, DG-N), the US Air Force Office of Scientific Research (AFOSR) under Award FA9550-16-1-0384 (FG-N), the CINV supported by the Millennium Scientific Initiative (P029-022-F) (DG-N) and Beca ANID 21221905 (IJ-D).

References

1. R. Moraga-Amaro, J. M. Jerez-Baraona, F. Simon, J. Stehberg, Role of astrocytes in memory and psychiatric disorders. *Journal of Physiology-Paris* **108**, 240–251 (2014).

2. D. R. Cotter, C. M. Pariante, I. P. Everall, Glial cell abnormalities in major psychiatric disorders: the evidence and implications. *Brain Res Bull* **55**, 585–95 (2001).

3. D. Ongur, W. C. Drevets, J. L. Price, Glial reduction in the subgenual prefrontal cortex in mood disorders. *Proc Natl Acad Sci U S A* **95**, 13290–5 (1998).

4. M. Banasr, R. S. Duman, Glial loss in the prefrontal cortex is sufficient to induce depressive-like behaviors. *Biol Psychiatry* **64**, 863–70 (2008).

5. M. A. Orlovsky, V. E. Dosenko, F. Spiga, G. G. Skibo, S. L. Lightman, Hippocampus remodeling by chronic stress accompanied by GR, proteasome and caspase-3 overexpression. *Brain Research* **1593**, 83–94 (2014).

6. Y. I. Sheline, C. Liston, B. S. McEwen, Parsing the Hippocampus in Depression: Chronic Stress, Hippocampal Volume, and Major Depressive Disorder. *Biological Psychiatry* **85**, 436–438 (2019).

7. D. F. Hermens, *et al.*, Hippocampal glutamate is increased and associated with risky drinking in young adults with major depression. *Journal of Affective Disorders* **186**, 95–98 (2015).

8. L. J. Zhu, *et al.*, Hippocampal nuclear factor kappa B accounts for stress-induced anxiety behaviors via enhancing neuronal nitric oxide synthase (nNOS)-carboxy-terminal PDZ ligand of nNOS-Dexras1 coupling. *J Neurochem* **146**, 598–612 (2018).

9. A. P. S. de Vasconcellos-Bittencourt, *et al.*, Chronic Stress and Lithium Treatments Alter Hippocampal Glutamate Uptake and Release in the Rat and Potentiate Necrotic Cellular Death After Oxygen and Glucose Deprivation. *Neurochem Res* **36**, 793–800 (2011).

10. A. S.-C. [DONG Su-Ping XU Chang, YUAN Ting-Ting, Hippocampal NMDA Receptor is involved in Chronic Stress Induced Depressive-Like Behaviors via SP-NK1 Receptor Pathway. *Acta Psychologica Sinica* **43**, 1045–1054 (2011).

11. P.-E. Lutz, *et al.*, Increased functional coupling of the mu opioid receptor in the anterior insula of depressed individuals. *Neuropsychopharmacol.* **46**, 920–927 (2021).

12. J. A. Orellana, *et al.*, Restraint stress increases hemichannel activity in hippocampal glial cells and neurons. *Front. Cell. Neurosci.* **9** (2015).

13. V. Abudara, *et al.*, The connexin43 mimetic peptide Gap19 inhibits hemichannels without altering gap junctional communication in astrocytes. *Frontiers in Cellular Neuroscience* **8**, 1–8 (2014).

14. J. Kang, *et al.*, Connexin 43 Hemichannels Are Permeable to ATP. *Journal of Neuroscience* **28**, 4702–4711 (2008).

15. Z. C. Ye, M. S. Wyeth, S. Baltan-Tekkok, B. R. Ransom, Functional hemichannels in astrocytes: A novel mechanism of glutamate release. *Journal of Neuroscience* **23**, 3588–3596 (2003).

16. I. Jiménez-Dinamarca, *et al.*, GABAergic Regulation of Astroglial Gliotransmission through Cx43 Hemichannels. *IJMS* **23**, 13625 (2022).

17. G. Quesseveur, *et al.*, Attenuated Levels of Hippocampal Connexin 43 and its Phosphorylation Correlate with Antidepressant- and Anxiolytic-Like Activities in Mice. *Front. Cell. Neurosci.* **9** (2015).

18. R. Pun, M. H. Kim, B. J. North, Role of Connexin 43 phosphorylation on Serine-368 by PKC in cardiac function and disease. *Front. Cardiovasc. Med.* **9**, 1080131 (2023).

19. T. Jeanson, *et al.*, Antidepressants Impact Connexin 43 Channel Functions in Astrocytes. *Front Cell Neurosci* **9**, 495 (2015).

20. H. Li, A. Guo, M. Salgado, J. C. Sáez, C. G. Lau, The connexin hemichannel inhibitor D4 produces rapid antidepressant-like effects in mice. *J Neuroinflammation* **20**, 191 (2023).

21. J. E. Rash, T. Yasumura, F. E. Dudek, J. I. Nagy, Cell-Specific Expression of Connexins and Evidence of Restricted Gap Junctional Coupling between Glial Cells and between Neurons. *The Journal of Neuroscience* **21**, 1983–2000 (2001).

22. J. Stehberg, *et al.*, Release of gliotransmitters through astroglial connexin 43 hemichannels is necessary for fear memory consolidation in the basolateral amygdala. *FASEB j.* **26**, 3649–3657 (2012).

23. S. Linsambarth, *et al.*, Astroglial gliotransmitters released via Cx43 hemichannels regulate NMDAR-dependent transmission and short-term fear memory in the basolateral amygdala. *The FASEB Journal* **36** (2022).

24. C. Meunier, *et al.*, Contribution of Astroglial Cx43 Hemichannels to the Modulation of Glutamatergic Currents by D-Serine in the Mouse Prefrontal Cortex. *J Neurosci* **37**, 9064–9075 (2017).

25. R. B. Price, *et al.*, International pooled patient-level meta-analysis of ketamine infusion for depression: In search of clinical moderators. *Mol Psychiatry* (2022). https://doi.org/10.1038/s41380-022-01757-7.

26. M. W. Sherwood, S. H. R. Oliet, A. Panatier, NMDARs, Coincidence Detectors of Astrocytic and Neuronal Activities. *IJMS* **22**, 7258 (2021).

27. E. Kartvelishvily, M. Shleper, L. Balan, E. Dumin, H. Wolosker, Neuron-derived D-Serine Release Provides a Novel Means to Activate N-Methyl-D-aspartate Receptors. *Journal of Biological Chemistry* **281**, 14151–14162 (2006).

28. M. Maugard, P.-A. Vigneron, J. P. Bolaños, G. Bonvento, l-Serine links metabolism with neurotransmission. *Progress in Neurobiology* **197**, 101896 (2021).

29. P. M. Kim, *et al.*, Serine racemase: Activation by glutamate neurotransmission via glutamate receptor interacting protein and mediation of neuronal migration. *Proc. Natl. Acad. Sci. U.S.A.* **102**, 2105–2110 (2005).

30. T. M. Ma, *et al.*, Serine Racemase Regulated by Binding to Stargazin and PSD-95. *Journal of Biological Chemistry* **289**, 29631–29641 (2014).

31. M. Popoli, Z. Yan, B. S. McEwen, G. Sanacora, The stressed synapse: the impact of stress and glucocorticoids on glutamate transmission. *Nat Rev Neurosci* **13**, 22–37 (2011).

32. W. N. Marsden, Stressor-induced NMDAR dysfunction as a unifying hypothesis for the aetiology, pathogenesis and comorbidity of clinical depression. *Medical Hypotheses* **77**, 508–528 (2011).

33. N. Wang, *et al.*, Selective inhibition of Cx43 hemichannels by Gap19 and its impact on myocardial ischemia/reperfusion injury. *Basic Res Cardiol* **108**, 309 (2013).

34. S. Liu, *et al.*, A structural basis for the unequal sensitivity of the major cardiac and liver gap junctions to intracellular acidification: the carboxyl tail length. *Biophysical Journal* **64**, 1422–1433 (1993).

35. M. Delmar, W. Coombs, P. Sorgen, H. S. Duffy, S. A. Taffet, Structural bases for the chemical regulation of Connexin43 channels. *Cardiovascular Research* **62**, 268–275 (2004).

36. O. Trott, A. J. Olson, AutoDock Vina: Improving the speed and accuracy of docking with a new scoring function, efficient optimization, and multithreading. *J. Comput. Chem.* NA-NA (2009). https://doi.org/10.1002/jcc.21334.

37. J. J. Irwin, T. Sterling, M. M. Mysinger, E. S. Bolstad, R. G. Coleman, ZINC: A Free Tool to Discover Chemistry for Biology. *Journal of Chemical Information and Modeling* **52**, 1757–1768 (2012).

38. J. J. Irwin, B. K. Shoichet, ZINC - A free database of commercially available compounds for virtual screening. *Journal of Chemical Information and Modeling* **45**, 177–182 (2005).

39. L. Z. Benet, C. M. Hosey, O. Ursu, T. I. Oprea, BDDCS, the Rule of 5 and drugability. *Advanced Drug Delivery Reviews* **101**, 89–98 (2016).

40. J. I. Nagy, D. Patel, P. A. Ochalski, G. L. Stelmack, Connexin30 in rodent, cat and human brain: selective expression in gray matter astrocytes, co-localization with connexin43 at gap junctions and late developmental appearance. *Neuroscience* **88**, 447–68 (1999).

41. K. A. Schalper, N. Palacios-Prado, J. A. Orellana, J. C. Sáez, Currently Used Methods for Identification and Characterization of Hemichannels. *Cell Communication & Adhesion* **15**, 207–218 (2008).

42. R. Lagos-Cabré, *et al.*, αVβ3 Integrin regulates astrocyte reactivity. *J Neuroinflammation* **14**, 194 (2017).

43. K. V. Raju, G. M. Gautam, V. R. Rao, Cacotheline as a redox indicator in the determination of antimony(V), thallium(III), osmium(VIII) and iridium(IV) with iron(II). *Analyst* **114**, 1293–1295 (1989).

44. J. J. Miguel-Hidalgo, *et al.*, Glial and glutamatergic markers in depression, alcoholism, and their comorbidity. *J Affect Disord* **127**, 230–40 (2010).

45. L. Deutschenbaur, *et al.*, Role of calcium, glutamate and NMDA in major depression and therapeutic application. *Progress in Neuro-Psychopharmacology and Biological Psychiatry* **64**, 325–333 (2016).

46. C. A. Zarate, *et al.*, A randomized trial of an N-methyl-D-aspartate antagonist in treatment-resistant major depression. *Arch Gen Psychiatry* **63**, 856–64 (2006).

47. C. Loo, *et al.*, Efficacy and safety of a 4-week course of repeated subcutaneous ketamine injections for treatment-resistant depression (KADS study): randomised double-blind active-controlled trial. *Br J Psychiatry* **223**, 533–541 (2023).

48. N. Kang, *et al.*, Astrocytes release d-serine by a large vesicle. *Neuroscience* **240**, 243–257 (2013).

49. Y. Pankratov, U. Lalo, Role for astroglial α1-adrenoreceptors in gliotransmission and control of synaptic plasticity in the neocortex. *Front. Cell. Neurosci.* **9** (2015).

50. M. Martineau, Gliotransmission: focus on exocytotic release of L -glutamate and D -serine from astrocytes. *Biochemical Society Transactions* **41**, 1557–1561 (2013).

51. J. T. Ehmsen, *et al.*, D-Serine in Glia and Neurons Derives from 3-Phosphoglycerate Dehydrogenase. *Journal of Neuroscience* **33**, 12464–12469 (2013).

52. D. T. Balu, S. Takagi, M. D. Puhl, M. A. Benneyworth, J. T. Coyle, d-Serine and Serine Racemase are Localized to Neurons in the Adult Mouse and Human Forebrain. *Cell Mol Neurobiol* **34**, 419–435 (2014).

53. K. Skowrońska, M. Obara-Michlewska, M. Zielińska, J. Albrecht, NMDA Receptors in Astrocytes: In Search for Roles in Neurotransmission and Astrocytic Homeostasis. *IJMS* **20**, 309 (2019).

54. N. Thirugnanasambandam, J. Grundey, W. Paulus, M. A. Nitsche, Dose-Dependent Nonlinear Effect of L-DOPA on Paired Associative Stimulation-Induced Neuroplasticity in Humans. *Journal of Neuroscience* **31**, 5294–5299 (2011).

55. J.-G. He, H.-Y. Zhou, F. Wang, J.-G. Chen, Dysfunction of Glutamatergic Synaptic Transmission in Depression: Focus on AMPA Receptor Trafficking. *Biological Psychiatry Global Open Science* **3**, 187–196 (2023).

56. J. D. Shepherd, R. L. Huganir, The Cell Biology of Synaptic Plasticity: AMPA Receptor Trafficking. *Annu. Rev. Cell Dev. Biol.* **23**, 613–643 (2007).

57. M. T. Lee, *et al.*, Neurobiology of Depression: Chronic Stress Alters the Glutamatergic System in the Brain—Focusing on AMPA Receptor. *Biomedicines* **10**, 1005 (2022).

58. J.-T. Pougnet, *et al.*, ATP P2X Receptors Downregulate AMPA Receptor Trafficking and Postsynaptic Efficacy in Hippocampal Neurons. *Neuron* **83**, 417–430 (2014).

59. U. Lalo, O. Palygin, A. Verkhratsky, S. G. N. Grant, Y. Pankratov, ATP from synaptic terminals and astrocytes regulates NMDA receptors and synaptic plasticity through PSD-95 multi-protein complex. *Sci Rep* **6**, 33609 (2016).

60. G. Cheung, *et al.*, Physiological synaptic activity and recognition memory require astroglial glutamine. *Nat Commun* **13**, 753 (2022).

61. G. Cheung, *et al.*, Astroglial Connexin 43 Regulates Synaptic Vesicle Release at Hippocampal Synapses. *Cells* **12**, 1133 (2023).

62. A. Panatier, *et al.*, Astrocytes Are Endogenous Regulators of Basal Transmission at Central Synapses. *Cell* **146**, 785–798 (2011).

63. M. Letellier, Y. Goda, Astrocyte Calcium Signaling Shifts the Polarity of Presynaptic Plasticity. *Neuroscience* **525**, 38–46 (2023).

64. G. Perea, A. Araque, Astrocytes Potentiate Transmitter Release at Single Hippocampal Synapses. *Science* **317**, 1083–1086 (2007).

65. S. Mahmoud, M. Gharagozloo, C. Simard, D. Gris, Astrocytes Maintain Glutamate Homeostasis in the CNS by Controlling the Balance between Glutamate Uptake and Release. *Cells* **8**, 184 (2019).

66. M. Navarrete, A. Araque, Endocannabinoids potentiate synaptic transmission through stimulation of astrocytes. *Neuron* **68**, 113–26 (2010).

67. A. Covelo, A. Araque, Neuronal activity determines distinct gliotransmitter release from a single astrocyte. *eLife* **7**, e32237 (2018).

68. B. Luscher, Q. Shen, N. Sahir, The GABAergic deficit hypothesis of major depressive disorder. *Mol Psychiatry* **16**, 383–406 (2011).

69. K. Ma, *et al.*, Impaired GABA synthesis, uptake and release are associated with depression-like behaviors induced by chronic mild stress. *Transl Psychiatry* **6**, e910–e910 (2016).

70. M. Li, X. Sun, Z. Wang, Y. Li, Caspase-1 affects chronic restraint stress-induced depression-like behaviors by modifying GABAergic dysfunction in the hippocampus. *Transl Psychiatry* **13**, 229 (2023).

71. Y.-T. Hu, Z.-L. Tan, D. Hirjak, G. Northoff, Brain-wide changes in excitation-inhibition balance of major depressive disorder: a systematic review of topographic patterns of GABA- and glutamatergic alterations. *Mol Psychiatry* **28**, 3257–3266 (2023).

72. B. E. Yoon, C. J. Lee, GABA as a rising gliotransmitter. *Front Neural Circuits* **8**, 141 (2014).

73. B.-E. Yoon, *et al.*, The amount of astrocytic GABA positively correlates with the degree of tonic inhibition in hippocampal CA1 and cerebellum. *Mol Brain* **4**, 42 (2011).

74. I. Srivastava, E. Vazquez-Juarez, L. Henning, M. Gómez-Galán, M. Lindskog, Blocking Astrocytic GABA Restores Synaptic Plasticity in Prefrontal Cortex of Rat Model of Depression. *Cells* **9**, 1705 (2020).

75. K. Ma, *et al.*, The molecular mechanism underlying GABAergic dysfunction in nucleus accumbens of depression-like behaviours in mice. *J Cellular Molecular Medi* **23**, 7021–7028 (2019).

76. A. Medina, *et al.*, Glutamate transporters: A key piece in the glutamate puzzle of major depressive disorder. *Journal of Psychiatric Research* **47**, 1150–1156 (2013).

77. P. F. Jacob, S. H. Vaz, J. A. Ribeiro, A. M. Sebastião, $P2Y_1$ receptor inhibits GABA transport through a calcium signalling-dependent mechanism in rat cortical astrocytes: GATs Modulation by $P2Y_1$ Receptor in Rat Astrocytes. *Glia* **62**, 1211–1226 (2014).

78. J. Lo, *et al.*, Activation of $P2X_7$ receptors decreases glutamate uptake and glutamine synthetase activity in RBA-2 astrocytes via distinct mechanisms. *Journal of Neurochemistry* **105**, 151–164 (2008).

79. M. Iwata, *et al.*, Psychological Stress Activates the Inflammasome via Release of Adenosine Triphosphate and Stimulation of the Purinergic Type 2X7 Receptor. *Biological Psychiatry* **80**, 12–22 (2016).

80. P. Illes, P. Rubini, H. Yin, Y. Tang, Impaired ATP Release from Brain Astrocytes May be a Cause of Major Depression. *Neurosci. Bull.* **36**, 1281–1284 (2020).

81. A. Araque, *et al.*, Gliotransmitters Travel in Time and Space. *Neuron* **81**, 728–739 (2014).

82. Z. Tan, *et al.*, Glia-derived ATP inversely regulates excitability of pyramidal and CCK-positive neurons. *Nat Commun* **8**, 13772 (2017).

83. H. Jiang, Y. Zhang, Z.-Z. Wang, N.-H. Chen, Connexin 43: An Interface Connecting Neuroinflammation to Depression. *Molecules* **28**, 1820 (2023).

84. M. Matos, *et al.*, Astrocytes detect and upregulate transmission at inhibitory synapses of somatostatin interneurons onto pyramidal cells. *Nat Commun* **9**, 4254 (2018).

85. D. N. Bowser, B. S. Khakh, ATP Excites Interneurons and Astrocytes to Increase Synaptic Inhibition in Neuronal Networks. *J. Neurosci.* **24**, 8606–8620 (2004).

86. T. Fellin, O. Pascual, P. G. Haydon, Astrocytes Coordinate Synaptic Networks: Balanced Excitation and Inhibition. *Physiology* **21**, 208–215 (2006).

87. O. Pascual, *et al.*, Astrocytic Purinergic Signaling Coordinates Synaptic Networks. *Science* **310**, 113–116 (2005).

88. A. Serrano, GABAergic Network Activation of Glial Cells Underlies Hippocampal Heterosynaptic Depression. *Journal of Neuroscience* **26**, 5370–5382 (2006).

89. A. J. Widman, L. L. McMahon, Disinhibition of CA1 pyramidal cells by low-dose ketamine and other antagonists with rapid antidepressant efficacy. *Proc. Natl. Acad. Sci. U.S.A.* **115** (2018).

90. A. Barbon, *et al.*, Regulation of Editing and Expression of Glutamate α-Amino-Propionic-Acid (AMPA)/Kainate Receptors by Antidepressant Drugs. *Biological Psychiatry* **59**, 713–720 (2006).

91. A. Barbon, *et al.*, Chronic antidepressant treatments induce a time-dependent up-regulation of AMPA receptor subunit protein levels. *Neurochemistry International* **59**, 896–905 (2011).

92. K. Zhang, *et al.*, Essential roles of AMPA receptor GluA1 phosphorylation and presynaptic HCN channels in fast-acting antidepressant responses of ketamine. *Sci. Signal.* **9** (2016).

93. A. Alt, E. S. Nisenbaum, D. Bleakman, J. M. Witkin, A role for AMPA receptors in mood disorders. *Biochemical Pharmacology* **71**, 1273–1288 (2006).

94. A. Pittaluga, *et al.*, Antidepressant treatments and function of glutamate ionotropic receptors mediating amine release in hippocampus. *Neuropharmacology* **53**, 27–36 (2007).

95. J. A. Orellana, M. A. Retamal, R. Moraga-Amaro, J. Stehberg, Role of Astroglial Hemichannels and Pannexons in Memory and Neurodegenerative Diseases. *Front Integr Neurosci* **10**, 26 (2016).

96. G. I. Gómez, *et al.*, Acute activation of hemichannels by ethanol leads to Ca2+-dependent gliotransmitter release in astrocytes. *Front. Cell Dev. Biol.* **12**, 1422978 (2024).

97. K. Maass, J. Shibayama, S. E. Chase, K. Willecke, M. Delmar, C-terminal truncation of connexin43 changes number, size, and localization of cardiac gap junction plaques. *Circ Res* **101**, 1283–91 (2007).

98. R. Ponsaerts, *et al.*, Intramolecular loop/tail interactions are essential for connexin 43-hemichannel activity. *FASEB j.* **24**, 4378–4395 (2010).

99. J. Gonzalez, *et al.*, NMDARs in neurological diseases: a potential therapeutic target. *The International journal of neuroscience* **125**, 315–27 (2015).

100. H. Li, *et al.*, Rifaximin-mediated gut microbiota regulation modulates the function of microglia and protects against CUMS-induced depression-like behaviors in adolescent rat. *J Neuroinflammation* **18**, 254 (2021).

101. C. A. Lipinski, Lead- and drug-like compounds: the rule-of-five revolution. *Drug Discovery Today: Technologies* **1**, 337–341 (2004).

102. C. A. Lipinski, F. Lombardo, B. W. Dominy, P. J. Feeney, Experimental and computational approaches to estimate solubility and permeability in drug discovery and development settings 1PII of original article: S0169-409X(96)00423-1. The article was originally published in Advanced Drug Delivery Reviews 23 (1997) 3–25. 1. *Advanced Drug Delivery Reviews* **46**, 3–26 (2001).

103. I. E. Alfaro, L. Varela-Nallar, M. Varas-Godoy, N. C. Inestrosa, The ROR2 tyrosine kinase receptor regulates dendritic spine morphogenesis in hippocampal neurons. *Molecular and Cellular Neuroscience* **67**, 22–30 (2015).

104. S. Kaech, G. Banker, Culturing hippocampal neurons. *Nat Protoc* **1**, 2406–2415 (2006).

Figures and Tables

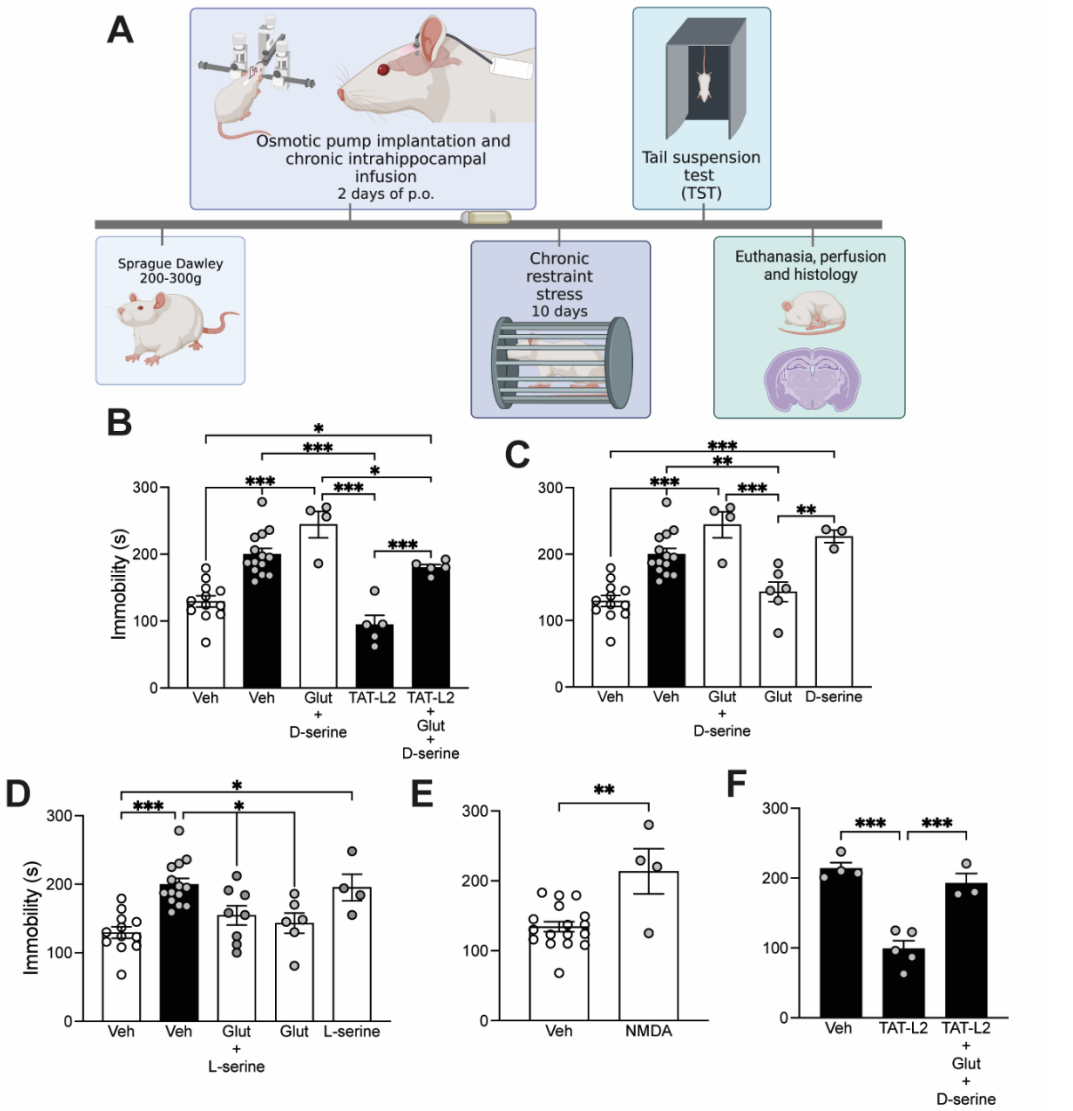

Figure 1. Cx43 hemichannel blockade in the ventral hippocampus during chronic restraint stress prevents the development of depressive-like symptoms, effect that is abolished by D-serine and glutamate. (**A)** Experimental design for cannula and osmotic pump implantation, chronic restraint stress and tail suspension test (TST). **(B)** Rats were subjected (black bar) or not (white bar) to 10 days of 2-h daily chronic restraint stress. The vehicle (Veh, black and white bars; n = 12, 14) or TAT-Cx43L2 (TAT-L2, 10nM, black bar; n = 5) were microinfused alone or with a mixture of 100mM glutamate and 200nM D-serine (TAT-L2 + Glu + D-ser, black bar; n=5 / Glu + D-ser, white bar n=5). **(C-E)** Rats without stress were chronically microinfused with a combination of glutamate and D-serine (Glu + D-ser, white bar; n=5), by each separately (Glu, white bar; n=5 / D-ser, white bar; n=5) **(C)**; glutamate (Glu, white bar; n=6), L-serine (L-ser, white bar; n=5), their combination (Glu + L-ser, white bar; n=8) **(D)**; and NMDAR agonist NMDA (NMDA; white bar; 2.71 mM, n=5) **(E)**. **(F)** Rats were chronically microinfused during chronic restraint stress with the vehicle (Veh, black bar; n = 18), TAT-L2 (black bar; n = 12) or TAT-L2 + glutamate and D-serine (TAT-L2 + Glu + D-ser,

black bar; n = 7), and tested 4 days after the end of stress (on day 18 from implantation). All microinfusions were performed bilaterally into the ventral hippocampus and evaluated on the TST the day after the end of stress (day 14 from implantation). *p<0.05, **p<0.01, ***p<0.001. Two-way ANOVA and Tukey *post-hoc* test.

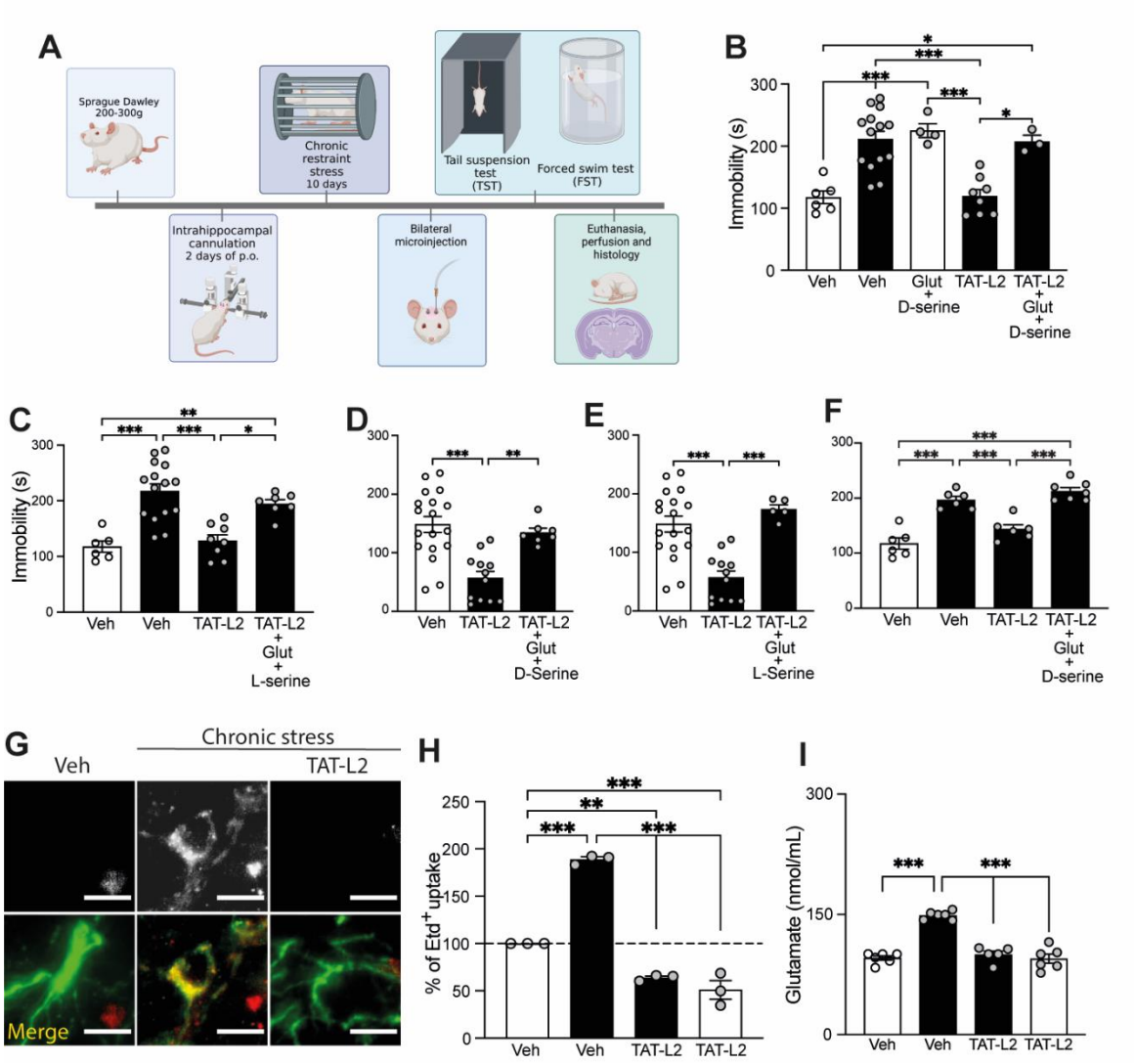

Figure 2. Acute Cx43 hemichannel blockade in the ventral hippocampus induces antidepressant effects in animals that previously underwent 10 days of chronic restraint stress, effect that is prevented by D-serine and glutamate. (**A)** Experimental design for cannula implantation, chronic restraint stress, acute bilateral microinjection and behavioral experiments; tail suspension test (TST) and forced swim test (FST). Rats were subjected (black bar) or not (white bar) to 10 days of 2h daily chronic restraint stress and on the day after the end of stress (Day 14 from implantation), were microinjected into their bilateral ventral hippocampus (vHipp) and their behavior was measured by TST or FST. **(B)** Animals acutely microinjected with vehicle (Veh, white and black bar; n = 6, 15) or 10 nM TAT-Cx43L2 peptide (TAT-L2, black bar; n = 8) alone or with a mixture of 100 mM glutamate and 200 nM D-serine (TAT-L2 + Glu + D-ser, black bar; n = 5 / Glu + D-ser, white bar n = 5), tested on the TST. **(C)** Rats acutely microinjected into the vHipp with vehicle (Veh, white and black bar; n = 6, 15) or TAT-L2 peptide (black bar; n = 8) alone or with a mixture of 100 mM glutamate and 200 nM L-serine (TAT-L2 + Glu + L-ser, black bar; n = 7) and their behavior was measured by TST. **(D)** Rats acutely microinjected into the vHipp with vehicle (Veh; n = 18) or TAT-L2

peptide (n = 12) alone or with a mixture of glutamate and D-serine (TAT-L2 + Glu + D-ser; n = 7) and their behavior was measured using the FST. **(E)** Rats were acutely microinjected into the vHipp with vehicle (Veh; n = 18), TAT-L2 alone (n = 12) or with a mixture of glutamate and L-serine (TAT-L2 + Glu + L-ser; n = 5) and their behavior was measured using the FST. **(F)** The antidepressant effects of intra-hippocampal TAT-L2 (n=6) were also found after chronic unpredictable mild stress (CUMS; black, white bars; no stress, n=7), compared to vehicle treated animals (black, Veh, n=6), effects that were prevented by co-infusion with glutamate and D-serine (TAT-L2+glutamate+D-serine, n=7). **(G)** Representative photomicrographs showing ethidium (Etd^+) uptake (red) in GFAP immuno-labeled cells (green) of hippocampal slices from rats subjected to 10 days of chronic restraint stress. TAT-L2 was used to corroborate Cx43 hemichannel-dependent uptake (n=3 per group), scale bar: 50 µm. **(H)** Quantification of Etd+ uptake in GFAP labeled astrocytes of ventral hippocampal slices obtained from animals that underwent (black bars) or not (white bars) 10 days of chronic restraint stress. Increased Etd^+ uptake was found in response to chronic restraint stress (veh, black bar) in comparison with non-stressed animals (veh, white bar). Etd^+ uptake was prevented by TAT-L2. **(I)** Increased extracellular glutamate (black bar) was found after chronic restraint stress in comparison with non-stressed control animals (white bar), which was prevented by preincubation with TAT-L2; n=3 per group. All behavioral tests were performed 30 min after bilateral intra-hippocampal microinfusions on the day after the end of stress (day 14 after implantation), *p<0.05, **p<0.01, ***p<0.001. Two-way ANOVA and Tukey *post-hoc* test.

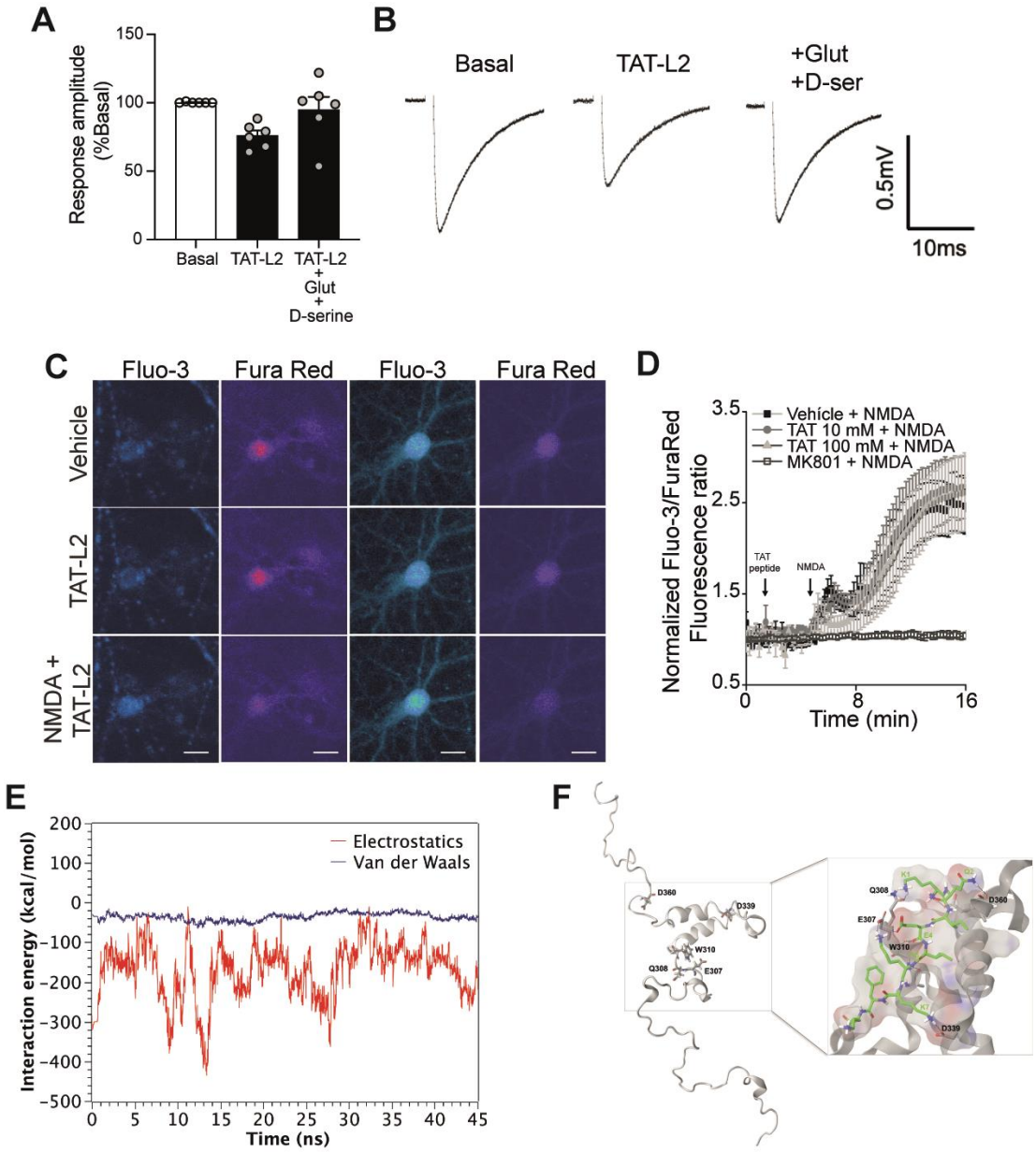

Fig. 3. TAT-Cx43L2 reduces postsynaptic NMDAR activity in the hippocampus on a glutamate- and D-serine- dependent manner. (A-B) TAT-Cx43L2 (TAT-L2, 10 nM) reduced postsynaptic NMDAR activity in rat ventral hippocampal slices, shown as percentage of basal fEPSP amplitude (n=4), effect that was prevented by addition of D-serine and glutamate. **(C)** TAT-L2 (100 μM) did not affect intracellular calcium responses of rat hippocampal cultured neurons to NMDA (50 μM), as seen in pseudo-colored images showing inverse changes in fluorescence intensity of Fluo-3 (left panel) and Fura-Red (right panel), scale bar: 50 μm. **(D)** Quantification of Fluo-3/Fura Red fluorescence ratios in function of time in response to TAT-L2 and NMDA. MK-801 was used as control of NMDAR inhibition. **(E)** TAT-L2/Cx43 CT interaction was modeled with Gap19, a shorter version of TAT-L2 peptide, via Molecular Dynamics for the complex. The energetic interaction of the complex during the simulation is shown; in red the

electrostatic interactions (-473 kcal/mol at 40 ns); in blue, the Van der Waals component of the interaction. **(F)** Prediction of GAP19-Cx43 C-terminal (CT) binding site using VMD software; the CT domain is shown in grey and GAP19 peptide is shown in green. Hydrogen bonds are represented as black dashed lines. *p<0.05, **p<0.01, one-way ANOVA, Bonferroni *post-hoc* test.

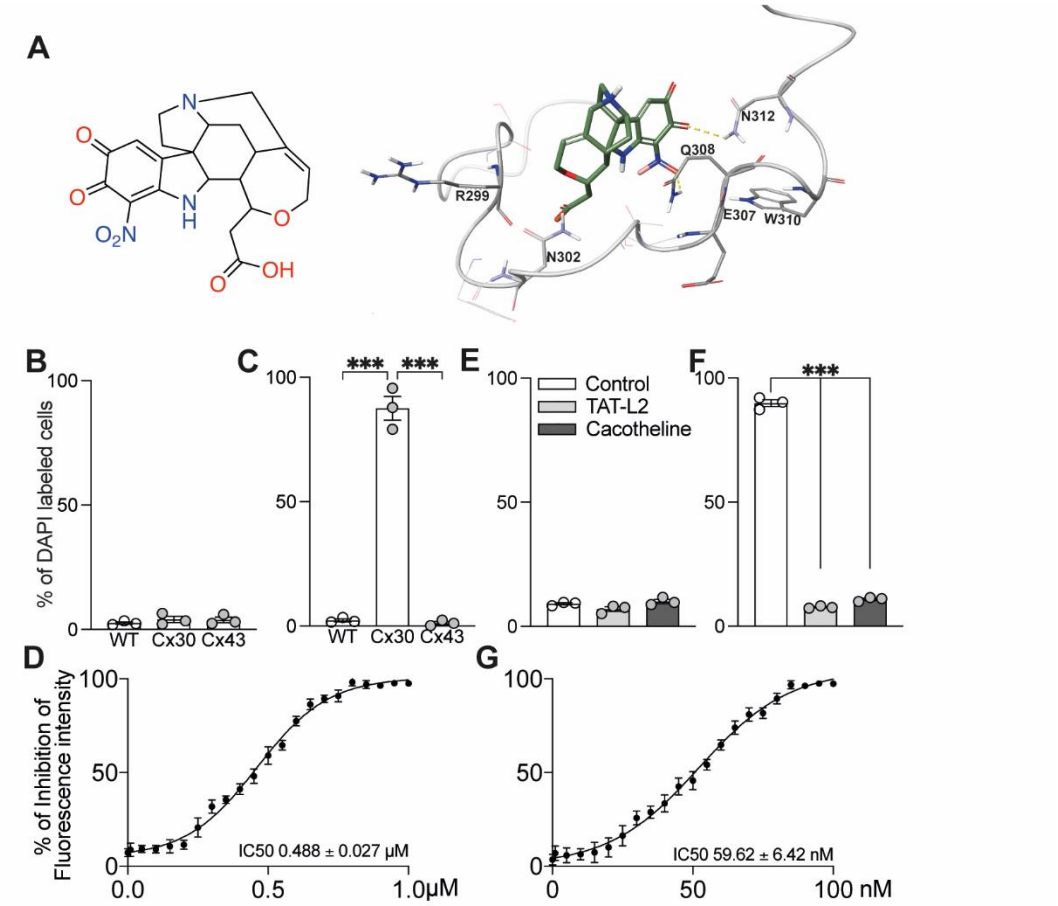

Figure 4. Blocking effects of cacotheline on Cx43 hemichannel activity in HeLa cells and the DI TNC1 rat astroglial cell line. (A) Chemical structure of cacotheline (left) and molecular docking for cacotheline with the Cx43 C-terminal (right) used to identify the relevant aminoacids for their interaction. **(B-C)** HeLa cells stably transfected with Cx43 and Cx30, were assayed for DAPI uptake in response to cacotheline 0.1 µM in the presence **(B)** or absence **(C)** of divalent cations in the culture medium. **(D)** IC50 for cacotheline (0.488 ± 0.027 µM) was calculated as percentage of inhibition of fluorescence intensity in HeLa cells transfected with Cx43. **(E–F)** Effects of 0.1 µM cacotheline and 10 nM TAT-Cx43L2 on DAPI uptake in the astroglial cell line DITNC1 in presence **(E)** or absence **(F)** of divalent cations in the culture medium. TAT-Cx43L2 and cacotheline induced similar uptake blocking effects. **(G)** The IC50 for cacotheline (59.62 ± 6.42 nM) in the astroglial cell line was calculated from DAPI uptake in response to varying concentrations of cacotheline. *p<0.05, **p<0.01, ***p<0.001. Two-way ANOVA with Tukey *post-hoc* test.

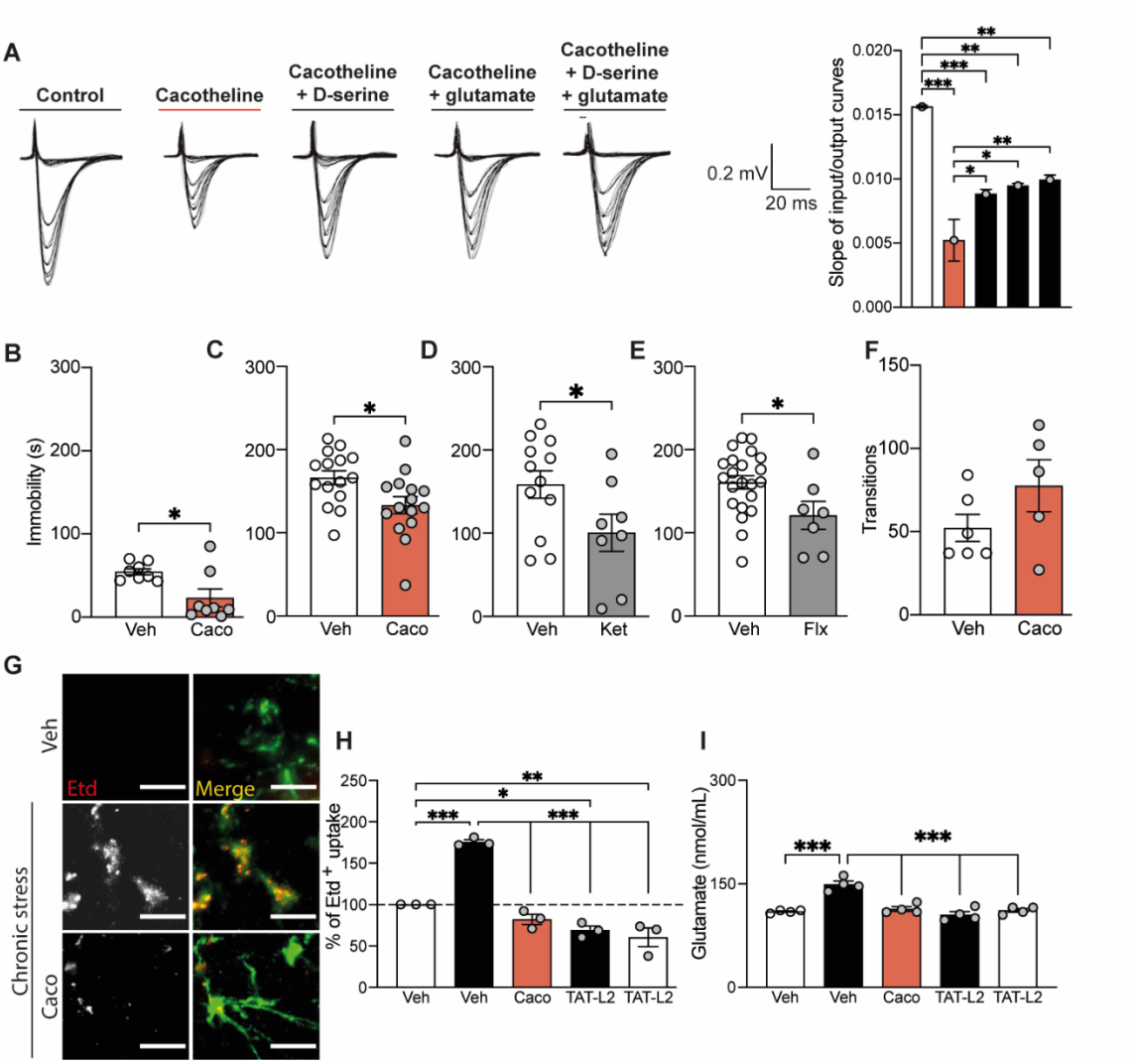

Figure 5. Cacotheline induces a reduction in dorsal hippocampal NMDAR activity which can be prevented by addition of D-serine and glutamate and has antidepressant effects when injected intraperitoneally. (A) Hippocampal slices were incubated with 1 µM cacotheline alone or with a mixture with glutamate, D-serine or both, and induced a reduction in NMDAR activity, with representative traces of fEPSPs(left) and their slope of input/output curves (right; n = 3). (**B-C**) A single dose of cacotheline (120 mg/kg) administered i.p. induced antidepressant-like effects on rats previously submitted to chronic restraint stress as measured using (**B**) tail suspension test (TST, n = 8), and (**C**) forced swim test (FST, n=15). (**D-E**) For comparison, the antidepressant effects of one dose of intraperitoneal subanesthetic ketamine (**D,** Veh, n = 12; Ket, 5,45 g/kg, n=8) and 21 days of fluoxetine in drinking water (**E,** Veh, n = 22; Flx, 0,7 mg/kg, n=8), measured using the TST. (**F**) Cacotheline did not affect locomotion as measured by transitions in the Open Field test (Veh, n = 7; Caco, n = 5). **(G)** Representative photomicrographs showing ethidium (Etd+) uptake (red) in GFAP labeled astrocytes (green) from hippocampal slices of animals subjected (black bars) or not (white bars) to chronic restraint stress for 10 days and administered i.p. with vehicle

(Veh) or cacotheline (Caco). **(H)** Quantification of Etd^+ uptake in ventral hippocampal slices, expressed as percentage of GFAP-labeled astrocytes showing Etd^+ uptake normalized to controls. Astroglial increase in Etd^+ uptake was found in response to chronic stress (black bar) compared to non-stressed controls (white bar), effect prevented by cacotheline treatment (Caco, red bar) and preincubation with TAT-Cx43L2 (TAT-L2, black bar), n=3 per group, scale bar: 50 µm. **(I)** Increased extracellular glutamate was found in the culture medium of hippocampal slices after chronic restraint stress (Veh, black) compared to non-stressed controls (Veh, white), which was prevented by i.p. cacotheline treatment (Caco, red bar), leading to glutamate levels similar to TAT-Cx43L2 preincubation (TAT-L2, black bar), n=3 per group, *p<0.05, **p<0.01, ***p<0.001. Two-way ANOVA and Tukey *post-hoc* test.

Supplementary Material

The role of astrocytes in depression, its prevention and treatment by targeting astroglial gliotransmitter release

Yorley Duarte[1†], Daisy Quintana-Donoso[2†], Rodrigo Moraga-Amaro[2], Ivanka Dinamarca[2], Yordan Lemunao[2], Kevin Cárdenas[2], Tamara Bahamonde[2], Tabita Barrientos[2], Pedro Olivares[1], Camila Navas[1], Francisco J. Carvajal[3], Yessenia Santibánez[2], Raimundo Castro-Lazo[2], María Paz Meza[2], Ramon Jorquera[4], Gonzalo I. Gómez[5], Marina Henke[6], Rodrigo Alarcón[7], Laureen A. Gabriel[6], Susanne Schiffmann[6], Waldo Cerpa[3], Mauricio A. Retamal[7], Felipe Simon[8-10], Sergio Linsambarth[2], Fernando Gonzalez-Nilo[1,11] and Jimmy Stehberg[1,2*]

Corresponding author: Jimmy Stehberg. jstehberg@unab.cl

Materials and Methods

All procedures involving animals were performed according to NIH guidelines and with approval of the Universidad Andrés Bello Bioethical Committee (Acta 030 – 2015). Sprague-Dawley rats (~60 d old, ~250 g) were caged individually at 22°C and a 12/12 h light/dark cycle. The rats remained in their homecages throughout the study and were removed only briefly, for drug microinfusions, intraperitoneal administration, or behavioral procedures.

Drugs for acute intra-hippocampal and systemic administration

For drug intra-hippocampal microinfusions, TAT-Cx43L2 (YGRKK RRQRRRKQIEIKKFK: Biomatik, Cambridge, Canada, >95% purity) was dissolved in PBS to yield a final solution of 10 nM. Glutamate (100 mM; SIGMA-ALDRICH) L-serine (200 nM; SIGMA-ALDRICH), D-serine (200 nM; SIGMA-ALDRICH) and NMDA (2.71 mM; SIGMA-ALDRICH) were dissolved in sterile saline. Cacotheline (2,3-Dihydro-4-nitro-2,3-dixo-9,10-secostrychnidin-10-oic acid; ZINC26730911), was purchased from TCI (Tokyo, Japan) and dissolved in PBS to yield a final concentration of 100 µM.

To evaluate systemic antidepressant-like effects, cacotheline was administered intra-peritoneally at 120 mg/kg, dissolved in PBS. Ketamine was injected intraperitonially at 5.45 g/kg dissolved in 0.9% saline (*50*). Control rats were injected with equal volumes of PBS or saline, respectively. Behavioral tests were performed 30 mins after administration of the compounds. Fluoxetine (Sigma-Aldrich) was administered in drinking water to yield a final daily dose of 0.7 mg/kg in 20 ml per rat, for 21 days. This dose has been previously shown to induce antidepressant effects in rats and to produce the same plasma level of fluoxetine than the 40 mg/day fluoxetine treatment for an average 60 kg person (*51*), which is recommended by the supplier (Prozac FDA Prospect, 2009).

Intra-hippocampal microinjection surgery for acute microinjections

The protocol was conducted as previously reported (*52*). Under ketamine/xylazine/acepromazine anesthesia (60.6 mg/kg; 0.6 mg/kg and 6.67 mg/kg, respectively), rats were stereotaxically implanted with bilateral 21-gauge stainless steel cannulas aimed 1.0 mm above the ventral hippocampus (coordinates:5.04 mm anterior to Bregma, 5 mm lateral to the midline, and -6 mm ventral to the skull surface). The cannulas were fixed with acrylic dental cement and secured by 4 skull screws. A stylus was placed inside the guide cannula to prevent clogging. Rats were given at least 7 days to recover before experimental procedures began. Pre surgical care included the application of a Bacitracin/Neomicin antideptic dermal cream (Laboratorio Chile) and post-surgical care included administration of a bolus of ketoprofen (3 mg/kg, Naxpet) and 100µl penicillin.

Intracerebral acute microinjections

In all experiments, the stylus was removed from the guide cannula and a 25-gauge injection cannula was inserted along the guide cannula, extending 1.0 mm beyond its tip into the ventral hippocampus. Drugs (0.5 µl) were infused into each hemisphere at a rate of 0.25 µl/min, via the injection cannula connected to Hamilton micro-syringes by PE20 tubing, driven by a micro-infusion pump. Following drug infusion, injection cannulas were left in place for 1 min to allow drug diffusion. Behavioral tests were performed 5 min after microinjection. All experimental groups were compared to a vehicle injected group to control for vehicle and volume effects.

Intra-hippocampal bilateral cannulation for chronic drug administration

For chronic intra-hippocampal administration, a 200µl osmotic pump (ALZET) was used per animal (compound release rate: 0.5 µl/hr, duration of 14 days), connected into a Y connector (Plastics One Inc, USA), which was connected via PE20 tubing into bilateral cannulas (30G). For implantation surgery, animals were anesthetized in a chamber with isoflurane and placed in the stereotaxic apparatus, maintaining isoflurane anesthesia (2.5% induction and 2.0% maintenance). Subcutaneous lidocaine was applied to the surface of the skull to later expose the skull surgically. Landmarks (lambda and bregma) were established, and the skull was drilled bilaterally for cannula implantation at the ventral hippocampus using the following coordinates: 5.04 mm posterior to Bregma; 5.0 mm lateral to the midline, and 6 mm ventral to the surface of the skull (Paxinos, 2007). Subsequently, the cannulas were fixed to the skull with dental cement (mixture of self-curing pink acrylic with methyl methacrylate monomer), secured by two screws to the skull surface. The cannulas were connected to the osmotic pump, which was implanted via a 1 cm

vertical incision on the dorsal part of the animal's neck, through which the skin was separated from the muscle using forceps and the osmotic pump was inserted subcutaneously. Finally, the incision was sutured, and a Bacitracin/Neomycin antiseptic skin ointment (Laboratorio Chile) was administered over the wound. At the end of the surgery, a single dose of the anti-inflammatory ketoprofen (3 mg/kg, Naxpet, Dragpharma, Chile) and a 100µl of a 1200000 IU penicillin solution to prevent infections, were administered subcutaneously. The animal had a postoperative recovery period of 48 h before the chronic restraint stress began.

Chronic restraint stress

To induce depressive-like symptoms, rats underwent the chronic restraint stress protocol, which consisted in placing each animal into a wire mesh cage (14 x 6 cm) for 2 h per day for 10 consecutive days before behavioral evaluations.

Chronic unpredictable mild stress

The CUMS procedure was performed as previously described (1) with a slight modification. Rats in the CUMS group were exposed to different stressors: cold swimming for 5 min (at 0 °C), water or food deprivation for 24 h, tail nip for 1 min (1 cm from the end of the tail), damp bedding, restraint for 2h and inversion of the light/dark cycle for 24 h. These stressors were applied for 28 days, during which each stressor was applied 4 times. The same stressor was not applied on consecutive days. Control rats were not subjected to stressors and kept on their home cages for the 28 days.

Behavioral evaluations

To evaluate depressive-like symptoms induced by chronic restrain stress, two tests were used: **1)** Tail suspension test (TST), in which rats are suspended above the ground by their tails, which are attached with tape to a suspension bar. The approximate distance between the rat's nose and the floor was set to 20-25 cm. The behavior was recorded for offline analysis while the animals were hanging for 6 mins and then released and returned to their homecages. Depressive-like symptoms were measured as increased immobility time (time that the animal ceased trying to escape, stopped trying to reach the walls of the apparatus or the suspension bar, stopped shaking or moving their limbs akin to running) and the time spent struggling, and compared to control non-stressed animals. **2)** Forced swim test (FST), in which rats are individually placed in a plastic cylinder (height 50cm, diameter 20cm) filled up to 33 cm with warm water (22±1°C). In the pre-test day, rats are placed in the setup for 15 min and the next day (test day), the animals are placed in the same cylinder for 5 min and their behavior is recorded for offline analysis. The parameter measured as depressive-like was an increase in immobility time (time floating without struggling to escape or climb up the cylinder) compared to non-stressed controls. The open field test was used to assess exploratory locomotion over a 5-minute period. This test was conducted using a transparent plexiglass box measuring 100 x 60 cm. A grid with 10 x 10 cm divisions was placed at the base of the box. The animals' behavior was recorded for subsequent offline analysis. The total distance traveled was quantified by counting the number of transitions, defined as the crossing of grid lines with all four paws.

Histology

At the end of the experiments, all animals were anesthetized with isoflurane and perfused intracardially with a saline solution followed by 4% paraformaldehyde buffered in PBS. The brains were extracted and post-fixed in 30% sucrose until their density equaled that of sucrose. Then the brains were sectioned using a cryostat, Nissl stained (Cresyl Violet) and examined with light microscopy for cannula placement and assessment of histological lesions as seen by tissue damage or gliosis. Animals with histological lesions beyond the size of the cannula tip or guide cannula diameter were excluded from the analysis. All behavioral experiments were performed blinded to the experimenter, and blinding was opened once the histological assessment was finished.

Hippocampal slice preparation and electrophysiology

Recordings were performed following a protocol reported previously (23). The animals were anesthetized with isoflurane as above and decapitated; their brains were rapidly removed and transverse slices (400 µm) from both dorsal and ventral hippocampi were cut in a cold ACSF solution which contained (in mM): (124) NaCl, (2.6) $NaHCO_3$, (10) D-glucose, (2.69) KCl, (1.25) KH_2PO_4 (2.5) $CaCl_2$, and (2.60) Na_2HPO_4, using a Vibratome (BSK microslicer DTK-1500E) and incubated in ACSF for 1 h at room

temperature. Slices were transferred to an experimental chamber (2 ml), superfused (3 ml/min, at room temperature) with gassed ACSF.

The ACSF for recording included 10 μM picrotoxin (PTX, Tocris) to suppress inhibitory $GABA_A$ transmission, 20 μM AMPAR antagonist NBQX (Tocris) to decrease AMPAR-dependent activity, and no Mg^{2+} to unblock NMDAR currents. Slices were visualized by trans-illumination with a binocular microscope (Amscope). To evoke field excitatory postsynaptic potentials (fEPSPs), bipolar concentric electrodes were used (Tungsten, 125 μm OD diameter, Microprobes) connected to an isolation unit (Isoflex, AMPI, Jerusalem, Israel). The stimulation was performed in the Stratum Radiatum within 100-200 μm from the recording site. Recordings were filtered at 2.0-3.0 kHz, sampled at 4.0 kHz using an A/D converter (National Instrument), and stored and analyzed using the WinLTP program. Basal excitatory synaptic transmission was measured using an input/output curve protocol of eight stimuli ranging from 200 to 900 μA, with a 10s interval between stimuli. Solutions of TAT-Cx43L2 (50 nM) with or without glutamate (10 μM) and D-serine (10 μM) for the ventral hippocampus, and TAT-Cx43L2 (50 nM) or cacotheline (1 μM) with or without glutamate (10 μM) and D-serine (10 μM) for the dorsal hippocampus, were added to the ACSF in the recording chamber. To control for potential combinatorial ordinal position effects, the slices were first incubated with TAT-Cx43L2, and then incubated either with glutamate and then D-serine, or D-serine and then glutamate. At the end of the recordings for the ventral hippocampus, 20μM of the NMDAR antagonist APV (SIGMA-ALDRICH) was used to corroborate that the recordings were from NMDAR currents. Data were collected and analyzed offline with pClamp 10 (Molecular Devices).

MD simulations

In order to study the potential structural interactions and dynamic stability between the Connexin 43 Carboxyl Terminal Domain (Cx43 C-terminal; PDB id: 1R5S) and both GAP19 and cacotheline, molecular dynamics simulations were run using the NAMD 2.7 software (*53*) in conjunction with the CHARMM36 force field, NPT ensemble, solvated in a box of water with the TIP3P water model, (*54*) with periodic boundary conditions at constant temperature (300°K) and pressure (1 atm). A solution of 0.15 mM of NaCl was added to ensure electrostatic neutrality, obtaining a final system size of 85.730 atoms. Minimization and balance were generated from the model with a 2000 ps simulation, bringing the system to a local energy minimum and ensuring adequate production dynamics. The data production for the system was obtained after 40 ns of simulation.

Virtual screening

The crystal structure of the Cx43 C-terminal (PDB id: 1R5S) was used for molecular docking. Prior to the virtual screening, Cx43 C-terminal was prepared by using *Molefacture* tool of the VMD (Visual molecular Dynamics) software (*55*), and it was subjected to a molecular dynamics simulation for relaxation. Once the molecular dynamics was concluded, the last frame was used for virtual screening. The molecule ZINC database (*23*) of commercially available ligand structures was used as the main source for screening. To identify novel putative Cx43 C-terminal modulators from the ZINC database (http://zinc.docking.org), molecular docking for 2,063,314 compounds was performed. The molecules tested were obtained in mol2 format, which comprises a representation of all atoms of the molecule, as well as the atomic partial charges and the order of atomic bonds. These molecules were prepared using the openbabel toolkit, (*56*) which calculates the partial charges of each atom, including the rotatable bonds as active twists and indicates the conformational degrees of freedom for the molecule. The state of protonation of the molecules were maintained as the 3D representation available in the ZINC database.

During the virtual screening, to parallelize calculations and optimize computation time, the files were organized into directories and the AutoDockVina software platform was employed for the calculations. From the *in-silico* modeling of the Cx43 C-terminal, the compounds that had the lowest binding score (highest theoretical affinity) to the Cx43 C-terminal domain were identified, and 1,000 of them were selected for the next step. The ADMET properties of the 1,000 compounds were predicted by Qikprop package (Schrödinger New York, NY, 2019). To select the best candidate compounds, two different drug-likeness criteria were used: logP, and Lipinski's rule of five; a total of 100 molecules were selected while taking into account these two parameters. These 100 molecules were searched in different libraries of molecules that were available, and a large number of those molecules were available at the National Cancer Institute of the USA (by request). Other compounds were obtained from other vendors. Cacotheline was obtained from TCI (Tokyo, Japan). A total of 65 molecules were obtained and tested *in vitro* using dye uptake.

DI TNC1 Astroglial cell culture

The rat astrocyte cell line DI TNC1 (ATCC CRL-2005) was cultured at 37°C and 5% CO_2 in Dulbecco's Modified Eagle's Medium (DMEM) supplemented with 5% fetal bovine serum (Life Technologies) and 100 µM/ml streptomycin/ampicillin (1:1, 100 IU/ml). The culture medium was replaced every other day.

Dye Uptake in Cx43 and Cx30 Expressing HeLa Cells and DIT NC1 Astrocytes

For visualization of dye uptake by snap-shot images, Cx30-, Cx43- stably transfected and WT HeLa cells at 80% of confluence were incubated with 4´,6-diamidino-2-phenylindole dihydrochloride (DAPI, Santa Cruz Inc., TX, USA) in 96 well plates with HEPES -buffered salt solution with calcium (140 mM NaCl, 4 mM KCl, 1 mM $CaC1_2$, 1 mM $MgC1_2$, 5 mM glucose, 10 nM HEPES) or bivalent cation free (140 mM NaCl, 4 mM KC1, 5 mM glucose, 2 mM EGTA, 10 nM HEPES). The compound cacotheline was added at two different concentrations (0.1 and 1 µM) to both solutions for 5 min, followed by 10 min of incubation with DAPI (10 µM). Cells were washed (to eliminate extracellular DAPI) and examined in fluorescence microscopy using a FLoid® Cell Imaging Station (Invitrogen, Eugene, OR). The same procedure was used for the astroglial cell line DI TNC1, with one difference; astroglial cells were incubated with DAPI (10 µM) for 5 min. Both the average fluorescence intensity per cell and the percentage of DAPI labeled cells were estimated. The percentage of DAPI labeled cells was quantified with respect to the total of cells visible under white light. To determine the IC50 of both TAT-Cx43L2 and cacotheline in HeLa cells and in the DI TNC1 cell line, the percentage of inhibition of fluorescence was plotted from uptake experiments using variable concentrations; from 10 nM to 1 µM for HeLa cells and from 1 nM to 100 nM for the DITNC1 cell line, and the concentration needed to attain a 50% inhibition was extrapolated.

Calcium imaging in hippocampal primary neuronal cell cultures

Cell culture isolation of mouse hippocampal neurons was prepared from C57BL6 mice at embryonic day 18 as described previously (2) and cultured at low density over a feeder layer of glia according to (3). For live-cell calcium imaging, hippocampal neurons were plated at low density of 8 × 10 3 cells/cm^2 in 40-mm cover slips pretreated with poly-l-lysine and cultured for 18-21 DIV. Hippocampal cells were loaded with the calcium-sensitive dyes Fluo-3 (5 µM) and Fura Red (15 µM) plus pluronic acid (0.02%) (Molecular Probes) for 30 min at 37°C, washed three times in ACSF plus HEPES (125 mM NaCl, 2.5 mM KCl, 26.2 mM $NaHCO_3$, 1 mM NaH_2PO4, 2.5 mM $CaCl_2$, 1.25 mM $MgCl_2$, 11 mM D-glucose, 25 mM HEPES) and placed in a closed-bath imaging chamber coupled to automated perfusion control (RC30WA chamber / VC6 valve system, Warner Instruments). Inverse responses to intracellular calcium and ratiometric measurements of Fluo-3 and Fura-Red fluorescence intensities allows accurate determination of the changes in calcium levels avoiding changes in fluorescence due to artifacts as focal drift and cell volume changes (4). Cells were continuously perfused at 0.5 ml/min with ACSF without Mg^{2+} for 5 min and then the medium was changed to ACSF without Mg^{2+} plus D-serine (100 µM) containing different concentrations of the TAT-Cx43L2 peptide (0, 10 and 100 µM) for 3 min to finally being stimulated with ACSF/D-serine without Mg^{2+} plus NMDA 50 µM. As a control of NMDAR inhibition, neurons were perfused with NMDAR antagonist MK-801 (Sigma-Aldrich) in ACSF/D-serine for 5 min before NMDA stimulation. Cells were imaged with an Olympus FV1200 confocal microscope with excitation at 488 nm and emissions were detected at 505–530 nm for Fluo-3 and with an LP650 filter for Fura Red. Images were acquired with a 20X air dry objective at 1024x1024 pixel resolution with intervals of 14 seconds. Fluo-3/Fura Red fluorescence intensity ratios in cell bodies of isolated neurons without evidence of potential remnant glial cells around neurons were analyzed using ImageJ imaging software and normalized to the mean of vehicle values. Between 20-30 neurons were analyzed per condition.

Dye uptake measurements in hippocampal slices

To obtain hippocampal slices, either naïve rats or rats that underwent 10 days of chronic restraint stress with or without the intraperitoneal administration of vehicle or cacotheline (120 mg/kg), were anesthetized under isoflurane, decapitated, their brains were extracted and cut into coronal slices (400 µm) in an ice-cold slicing solution containing (in mM): sucrose (222); KCl (2.6); $NaHCO_3$ (27); $NaHPO_4$ (1.5); glucose (10); $MgSO_4$ (7); $CaCl_2$ (0.5) and ascorbate (0.1), bubbled with 95% O_2/5% CO_2, using a vibratome (Leica, VT1000GS; Leica, Germany). Then, the slices were transferred to a holding chamber filled with artificial cerebral spinal fluid (ACSF), at room temperature (20-22°C), containing (in mM): 125 NaCl, 2.5

KCl, 25 glucose, 25 $NaHCO_3$, 1.25 NaH_2PO_4, 2 $CaCl_2$, and 1 $MgCl_2$, bubbled with 95% O_2/5% CO_2, pH 7.4, for a stabilization period of 60 min before dye uptake experiments.

Dye uptake ex vivo "snapshot" assays were performed as reported previously (20). The hippocampal slices (either from ventral or dorsal hippocampus) were incubated with 5 µM ethidium (Etd^+) for 10 min in a chamber oxygenated by bubbling 95% O_2/5% CO_2 into ACSF. To ascertain that the dye-uptake was mediated by Cx43 hemichannels, some of the slices were preincubated with 10 nM TAT-Cx43L2 for 10 min and then Etd^+ was added for another 10 min. After the exposure to Etd^+, the slices were washed three times with ACSF and were fixed at room temperature with 4% saccharose in 4% paraformaldehyde for 60 min, rinsed once for 5 min with 0.1 mM glycine in PBS, and then twice with PBS for 10 min with gentle agitation. Then the slices were sectioned using a cryostat to obtain ~ ten sections (40µm each). The sections from the slices were incubated twice for 30 min each with a blocking solution (PBS, gelatin 0.2%, Triton-X 100 1%) at room temperature and then incubated overnight at 4°C with a cell-specific antibody to identify astrocytes (anti-GFAP monoclonal antibody; Sigma-Aldrich). After the incubation with the antibody diluted 1:1,000 in the blocking solution, the slices were washed for 10-min with blocking solution, 3 times. The sections were then incubated for 2 h at room temperature with donkey anti-mouse Alexa Fluor 488 antibody (1:1,000, Abcam) and after 3 washes (10-min each), the slices were mounted in Fluoromount, cover-slipped and examined in an epifluorescence microscope (Nikon ECLIPSE Ti-E). Stacks of consecutive images were taken with a 60X objective at 1-µm intervals, acquired sequentially at two wavelengths (488 nm and 543 nm), and Z stack projections were reconstructed using ImageJ software (National Institute of Health, USA). Dye uptake was calculated as: corrected total cell Etd fluorescence intensity (as arbitrary units [AU]) = integrated density – ([area of selected cell] x [mean fluorescence of background readings]). At least six cells per field were selected from at least three fields in each brain slice. The background fluorescence was set as the average value of intensity in three regions of interest (ROI) void of any fluorescence.

To measure fluorescence intensity, ROIs in GFAP positive cells (astrocytes) were set surrounding cell nuclei and the fluorescent intensity was measured using ImageJ for each cell, for all cells in each quadrant, from the same quadrants that were analyzed for counting DAPI labelled cells (N=3 with triplicates). Fluorescent intensities were plotted for all fluorescence labeled cells, and the median number of labeled cells and median fluorescence were compared for each condition.

Measurement of extracellular glutamate from hippocampal slices

The hippocampal slices were obtained as above, but instead of adding Etd^+, the ACSF medium in which the slices were incubated was removed and transferred to 1 ml aliquots and frozen at -20°C. Extracellular glutamate levels were determined using a colorimetric enzyme-linked assay (Sigma-Aldrich). In the presence of glutamate dehydrogenase (GDH) and β-nicotinamide adenine dinucleotide phosphate ($NADP^+$), glutamate is oxidized to α-ketoglutarate, yielding NADPH, which can be determined fluorometrically for indirect quantification of glutamate concentration (excitation and emission wavelengths of 355 nm and 460 nm, respectively). For each assay, standard curves were constructed using standardized glutamate concentrations used to estimate the concentrations of glutamate in the samples, which are shown per mL of ACSF.

Single cell electrophysiology for hemichannel activity

HeLa cells transfected with Cx43 were cultured to 60-70% confluence in DMEM 10% fetal bovine serum, were washed with PBS twice and then detached from the culture well (60 mm - Nunc) with trypsin (TryPle express - Gibco) for 1-2 min at 37°C. Then, the cells were visualized in a light microscope to confirm that they had detached. The cells were then harvested and placed in a 15 ml tube, to which 2 ml of medium with serum was added to inactivate the trypsin. The cells were centrifuged for 2 min at 1500 rpm, the medium was discarded, and the cells were re-suspended in recording medium (in mM; NaCl [140], KCl [*31*], $MgCl_2$ [*31*] $CaCl_2$ [2], D-Glucose [5] and HEPES [10], pH 7.42). They were then centrifuged once more, the supernatant removed and then resuspended in 300 µl of recording medium and finally placed in a 1.5 ml Eppendorf tube. The cells were left at room temperature in the recording medium for 1 h to recover from the trypsinization procedure before using them for the electrophysiology experiments.

For electrophysiology, recordings were performed using the Nanion (Port-a-Patch). Six µl of a medium containing (in mM); NaCl (10), KCl (50), KF (*31*), EGTA (20), and HEPES (10), at a pH 7.42, were placed in the lower part of the registration chip (3-5 Mohm). Then, 6 µl of the medium was placed in the upper part of the registration chip, and then the chip was placed in the recording chamber. After this, 6-8 µl

of cells in suspension were placed in the upper part of the registration chip. Once the equipment detected a cell in the nano-orifice of the recording chip, it automatically modified both the pressure and the membrane potential of the cell to generate a Giga Ω seal. To improve this process, 20 µl of an enhancer solution containing (in mM): NaCl (80), KCl (3), MgCl (10), CaCl (35), and HEPES (10), at pH 7.42, were added.

Surface plasmon resonance (SPR)

SPR interaction analyses were performed using a Biacore T200 (GE Healthcare Life Sciences). SPR measurements were carried out in an HBS-N buffer (GE Healthcare) alone for the case of TAT-Cx43L2 and containing additionally 2% DMSO in case of cacotheline. Stock solutions were diluted in the same buffer. Data were analyzed using the BIA evaluation software (Biacore AB, Freiburg). Experiments were performed by monitoring the refractive index changes as a function of time under a constant flow rate of 10 µl/min. The relative amount of compound binding to the Cx43 protein was determined by measuring the net increase in refractive index over time compared to control running buffer. This change is usually reported in response units (RU). There is an inline subtraction of reference surface during the run. For the determination of the KD values, TAT-Cx43L2 and cacotheline were evaluated at various concentrations (0, 0.0001, 0.0001, 0.001, 0.01, 0.1, 1, 10 µM). Regeneration was carried out with 10 mM glycine-HCl at pH 2.5 for 30 s and at 30 µl/min.

Astroglial primary cultures

Astroglial primary cultures were prepared from brains of 1-2-day-old neonatal C57BL6 mice. Newborns were anesthetized using isoflurane and decapitated. Cortices were minced and incubated with 2.5% trypsin-EDTA in Hanks' solution (in g/L: 0.4 KCl, 0.06 KH_2PO_4, 0.048 Na_2HPO_4, 8 NaCl, 1 d-glucose, 2.4 HEPES and 3.5 $NaHCO_3$) for 15 min and mechanically dissociated. Cells were seeded in 75-cm^2 culture flasks in glial medium (MEM, 10% Horse Serum, 0.6% glucose, 100 units/ml penicillin, and 100 µg/ml streptomycin) and incubated at 37 °C in a water-saturated atmosphere with 5% CO_2. After 7-14 days of culture, the astrocytes were trypsinized, yielding a highly enriched astrocyte culture (>95% astrocytes).

Dye Coupling

The technique of Scrape Loading/Dye Transfer was used to measure the gap junctional intercellular communication between astrocytes, following previously reported protocols (19). Astrocytes from astroglial primary cultures were grown in a glass coverslip, and on the day of the experiment, each coverslip was placed in a 35 mm plastic dish and washed three times with a divalent cation free solution (DCFS, in mM: 140 NaCl, 4 KCl, 5 EGTA, 5 glucose, and 10 HEPES, pH = 7.4). Then, scrape was performed with a razor blade in the same DCFS containing 500 mM carboxyfluorescein (CF, Merck). After 20 min at room temperature, cells were washed at least six times with recording media (in mM: 140 NaCl, 4 KCl, 2 $CaCl_2$, 1 $MgCl_2$, 5 glucose, and 10 HEPES, pH = 7.4) to wash out the remaining CF. Images were captured using an inverted fluorescent microscope equipped for epifluorescence (Eclipse Ti-U, Nikon) and the NIS elements advanced research software (version 4.0, Nikon) was used for data acquisition and image analysis. Three images of different fields were taken for each cover and analyzed for dye transfer from cells along the edge of the cut, onto neighboring cells located further from the edge.

Data Analysis

Data are expressed as Mean ± SEM, unless stated otherwise. The data from the different experiments were tested for normality. For multiple comparisons, if the data was normally distributed, the statistical differences were assessed by a two-way analysis of variance (ANOVA), followed by Bonferroni *post hoc* test, and when comparing only 2 groups, unpaired student's t-test was used. When data was not found to be normally distributed, the Kruskal-Wallis test was used or the Wilcoxon test, as appropriate. Differences were considered significant when $p<0.05$. Only the p-values are written in the text and shown in the figures as either $p^{***}<0.001$, $p^{**}<0.01$ or $p^{*}<0.05$. Given the large amount of data, all averages, SE, statistical tests and results and p values were not included in the text but can be found in **Supplementary Table 1**.

Supplementary Figures

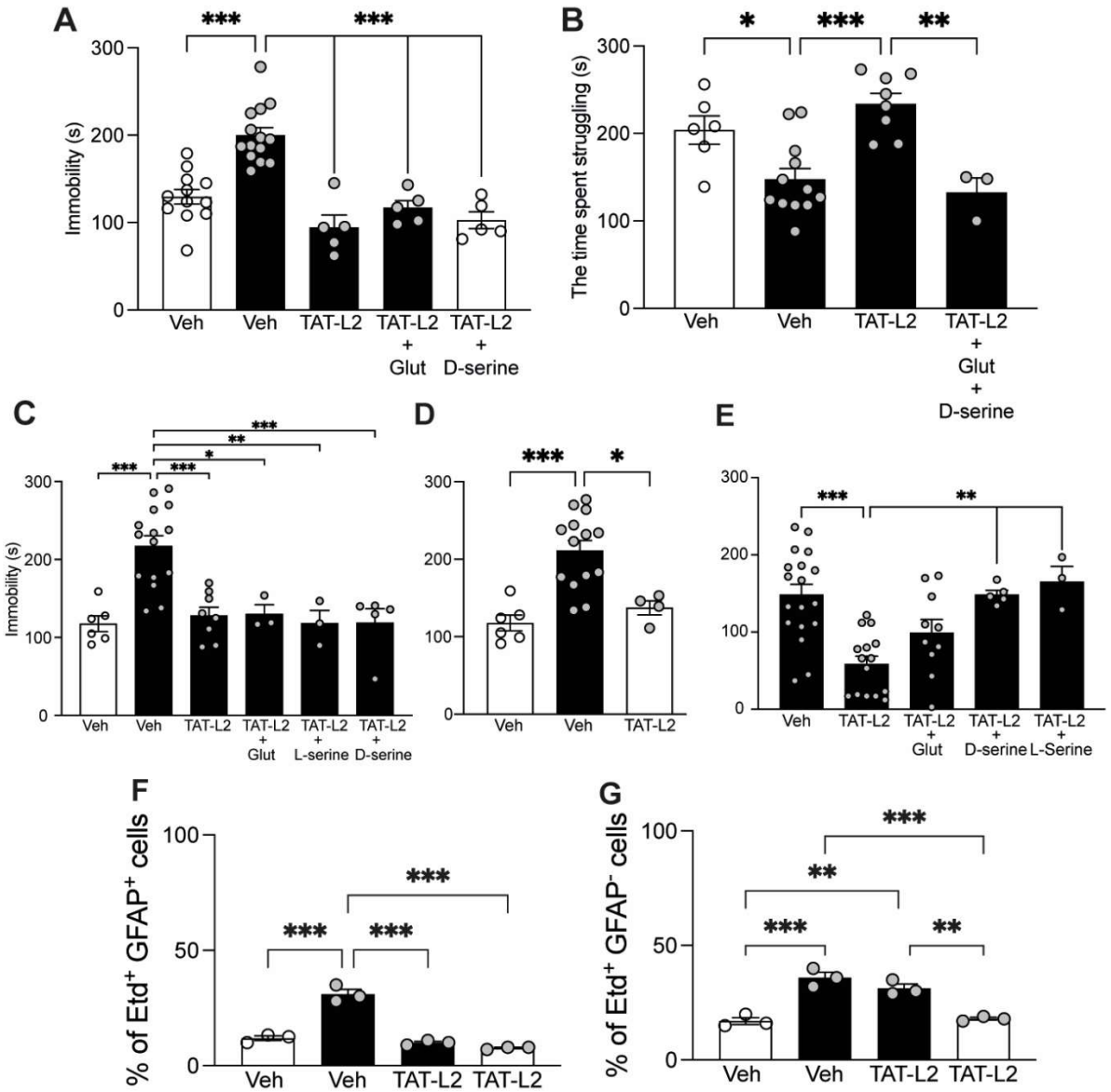

Figure S1. Controls for *in vivo* experiments. (A-B) Rats were subjected (black bar) or not (white bar) to chronic restraint stress for 10 days while being microinfused chronically with different drugs into the ventral hippocampus on day 11. Their depressive-like symptoms were measured in the TST by immobilization time **(A)** and by time struggling **(B)** on the day after the end of stress. Vehicle (Veh, white and black bars; n = 6, 15) or TAT-Cx43L2 were microinfused alone (TAT-L2, black bar; n = 8) or with glutamate (TAT-L2 + Glu, black bar, n = 5) or D-serine (TAT-L2 + D-ser, black bar, n = 5). **(C)** Rats that underwent chronic restraint stress (black bars) or not (white bars), on the day after the end of stress, were acutely microinjected with the vehicle (Veh, n = 18; TAT-Cx43L2; TAT-L2, n = 15; TAT-L2 + Glu, n = 10; TAT-L2 + D-ser, n = 5; TAT-L2 + L-ser, n = 5) and depressive-like symptoms were measured using the TST. **(D)** Rats that underwent chronic restraint stress (black bars) or not (white bars), on the day after the end of stress, were acutely microinjected with vehicle (Veh, white and black bar; n = 6, 15) or TAT-Cx43L2 peptide (TAT-L2, black bar; n = 8) and the time of immobility was measured in the TST eight days after the last stress (day 18). **(E)** Rats that underwent chronic restraint stress (black bars) or not (white bars), on the day after the end of stress, were acutely microinjected with the vehicle (Veh, white and black bars; n = 12, 14), TAT-Cx43L2

alone (TAT-L2, black bar; n = 5) or with glutamate (TAT-L2 + Glu,black bar, n = 5), D-serine (TAT-L2 + D-ser, black bar, n = 5) and depressive-like symptoms were measured using the FST. **(F)** Quantification of Etd+ uptake, expressed as percentage of GFAP labeled cells showing Etd+ uptake/ total number of cells with Etd+ uptake, n=3. **(G)** Quantification of Etd+ uptake, expressed as percentage of non-GFAP labeled cells showing Etd+ uptake/ total number of cells with Etd+ uptake, n=3; *p<0.05, **p<0.01, ***p<0.001. Two-way ANOVA with Tukey *post-hoc* test.

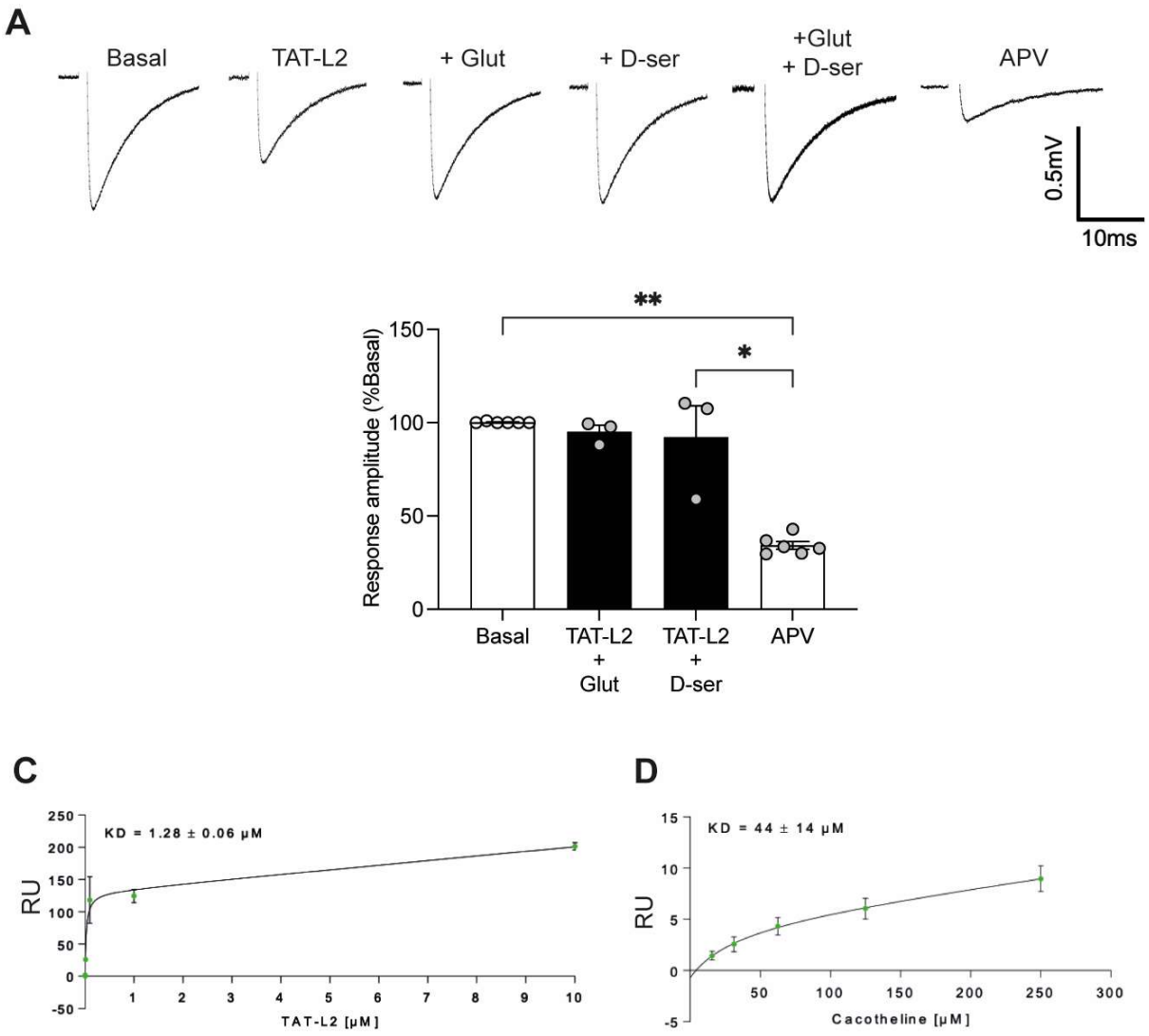

Figure S2. TAT-Cx43L2 effects on postsynaptic NMDAR and KD of the interaction between a synthetic Cx43 C-terminal and both TAT-Cx43L2 and cacotheline, measured using surface plasmon resonance. (A-B) Rat hippocampal slices were incubated with TAT-Cx43L2 in addition to glutamate or D-serine and field excitatory postsynaptic potential (fEPSP) amplitude was measured for NMDAR-dependent currents. **(C)** Concentration curve and KD value for TAT-Cx43L2 interactions with a synthetic Cx43 C-terminal, measured using surface plasmon resonance **(D)** Concentration curve and KD value for cacotheline interactions with a synthetic Cx43 C-terminal, measured using surface a plasmon resonance assay.

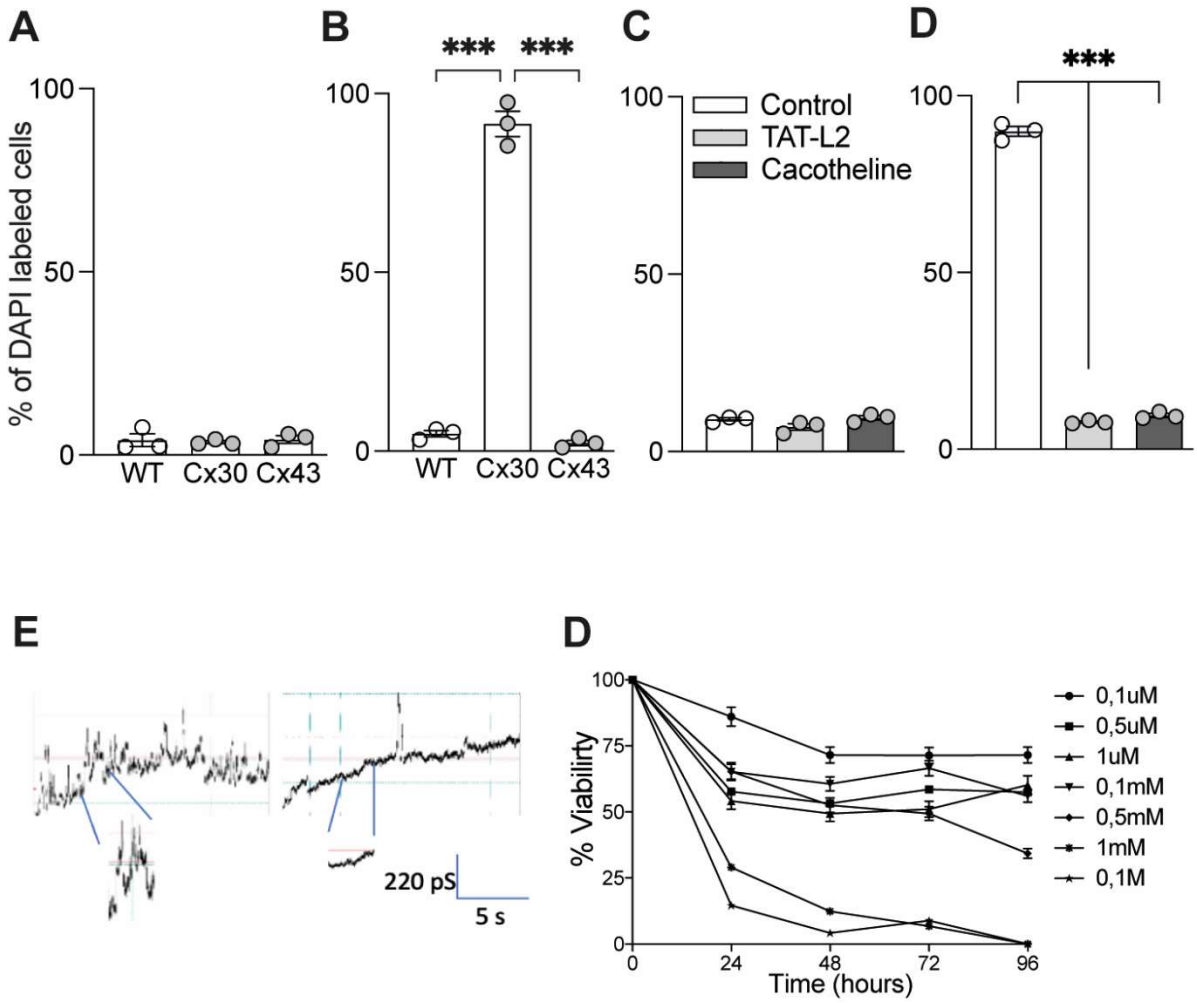

Figure S3. Cx43 and Cx30 hemichannel activity in Cx30- and Cx43-expressing HeLa cells, Cx43 hemichannel activity in DIT NC1 astrocytes and cell viability assay for cacotheline in Cx43-expressing HeLa cells. (A) HeLa cells transfected with Cx43 and Cx30, were assayed for DAPI uptake in presence **(B)** or absence **(A)** of divalent cations in response to cacotheline 1 µM. **(C – D)** Astroglial cell line DITNC1 was tested for DAPI uptake in presence **(C)** or absence **(D)** divalent cations in response to cacotheline 1 µM. **(E)** Blocking effects of cacotheline on Cx43 hemichannels conductance by patch clump electrophysiological recordings of single Cx43 transfected HeLa cells. **(F)** Cell viability assay (3-(4,5-Dimethylthiazol-2-yl)-2,5-Diphenyltetrazolium Bromide, MTT) performed at different concentrations, from 0.1 µM to 100 mM of cacotheline, at variable times (0 to 96 h), n = 3; *p<0.05, **p<0.01, ***p<0.001. Two-way ANOVA with Tukey *post-hoc* test.

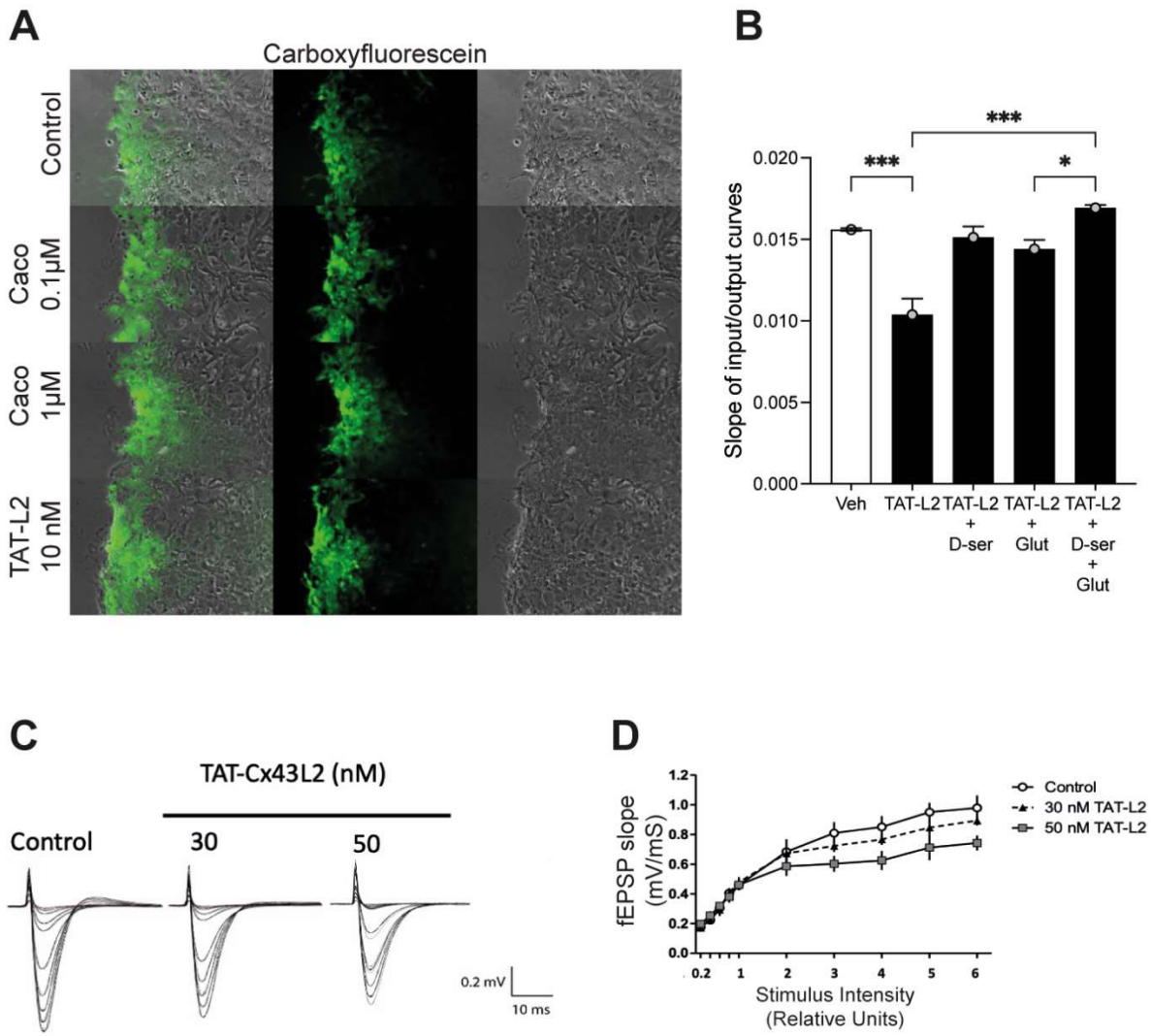

Figure S4. Effect of TAT-Cx43 L2 and cacotheline on astroglial Cx43 gap junctional coupling in primary astroglial culture and on postsynaptic NMDAR activity in the dorsal hippocampus. (A) Dye coupling assay in primary astroglial cultures for 10 nM TATCx43-L2 (TAT-L2), and for 0.1 µM and 1 µM cacotheline (Caco) **(B)** TAT-Cx43L2 induced a decrease in NMDAR activity in rat hippocampal slices as can be observed in fEPSP slope, which was prevented by addition of D-serine and glutamate and induced a reduction in NMDAR activity. Rat dorsal hippocampal slices were incubated with two doses of TAT-Cx43L2 (30nM and 50 nM). NMDAR-dependent currents were analyzed and representative traces of fEPSPs **(C)** and their slope **(D)** are shown.

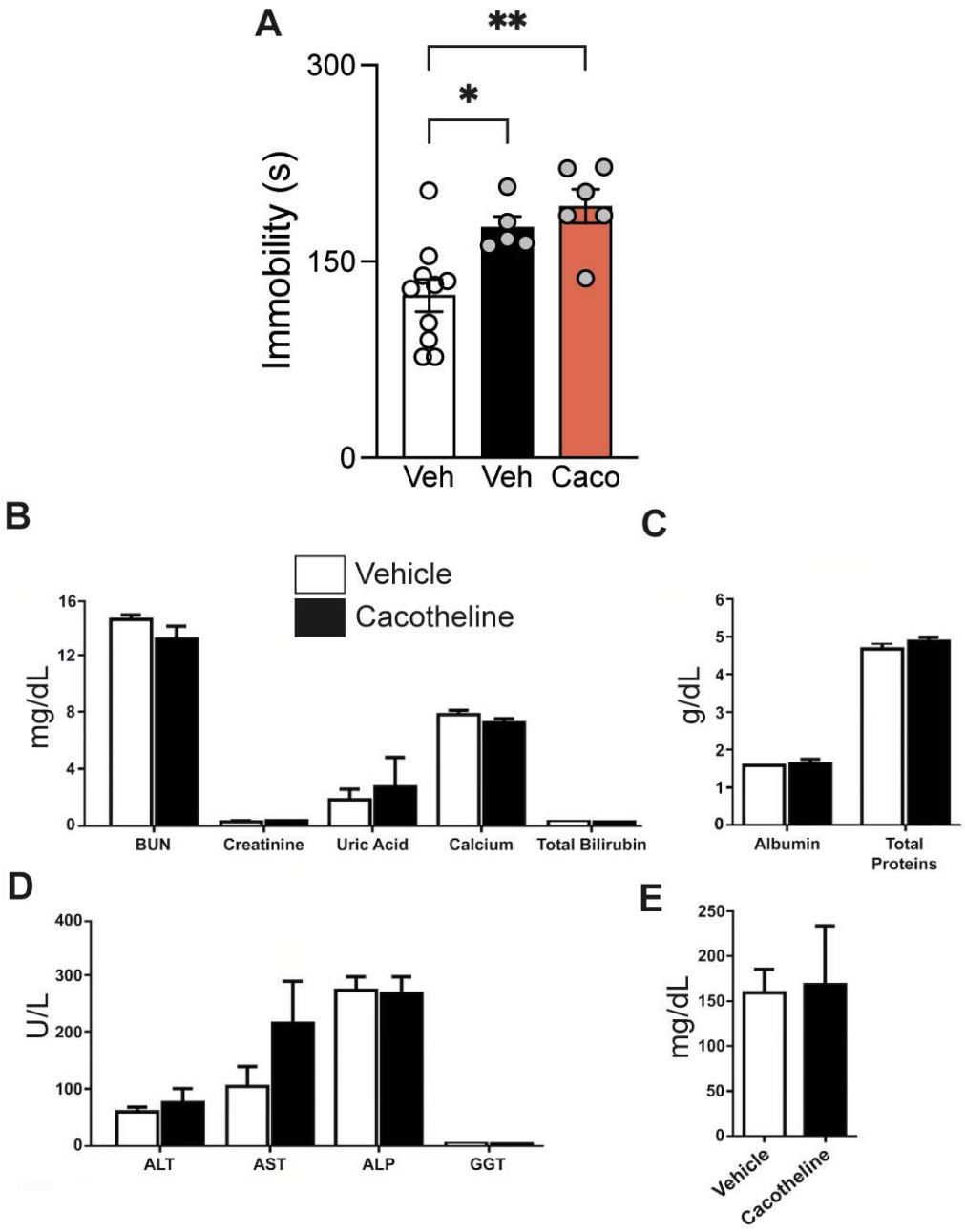

Figure S5. Effect of cacotheline on organ function. **(A)** Acute i.p. administration of cacotheline at 120 mg/kg to rats had no effects 7 days after the last stress (day 18) as measured using the TST **(B-E)** and had no effects on organic function as assessed by levels of renal and hepatic function markers. **(B)**. Comparison of analytes implicated in renal function (BUN, creatinine, uric acid, calcium) and hepatic function (total bilirubin). BUN: blood uric nitrogen. **(C)** Albumin and total serum proteins. **(D)** Transaminases (ALT, AST, GGT) and phosphatases (ALP) implied on hepatic function (ALT: Alanine-aminotransferase. AST: aspartate-aminotransferase. GGT: γ-Glutamil-transferase. ALP: alkaline phosphatase). **(E)** Glycemia comparison between controls and cacotheline injected rats. Statistical differences were assessed by t-test between vehicle (open bars) and cacotheline (closed bars) -treated animals. There were no significant differences between groups. Average data are shown ± SE, n=3 per group.

Table S1. Results: data and statistics

Figure 1. Chronic Cx43 hemichannel blockade in the ventral hippocampus prevents the development of depressive-like symptoms, which can be abolished by D-serine and glutamate.				
TST in rats with or without chronic restraint stress and chronic microinfusion (**Figure 1B**)				
Treatment	Immobility (s)	Comparison (One way ANOVA) ("– "compared groups)	Significance	n
Veh without stress	129.4 ± 8.35			12
Veh with stress	199.9 ± 8.69	Veh without stress – Veh with stress – TAT-L2	***	14
Glut + D-serine	244.3 ± 19.63	Veh without stress – Glut + D-serine – TAT-L2	***	4
TAT-L2	94.60 ± 13.99	Veh without stress – TAT -TAT + Glut + D-serine	***	5
TAT+ Glut + D-serine	180.2 ± 4.44	Veh without stress – TAT + Glut + D-serine Veh without stress – Glut + D-serine	*** *	5
TST in in chronic restraint stress and non-stressed rats with chronic microinfusion of glutamate or D-serine **(Figure 1C)**				
Treatment	Immobility (s)	Comparison (One way ANOVA) ("– ", compared groups)	Significance	n
Veh without stress	129.4 ± 8.35			12
Veh with stress	199.9 ± 8.69	Veh without stress – Veh with stress	***	14
Glut + D-serine	244.3 ± 19.63	Veh without – Glut + D-serine	***	4
Glut	143.3 ± 14.85	Veh with stress – Glut Glut + D-serine – Glut	** ***	6
D-serine	226.7 ± 9.35	Veh without stress – D-serine Glut – D-serine	*** **	3
TST in chronic restraint stress and non-stressed rats with chronic microinfusion of glutamate or L-serine (**Figure 1D**)				
Treatment	Immobility (s)	Comparison (One way ANOVA) ("– " compared groups)	Significance	n
Veh without stress	129.4 ± 8.35			12
Veh with stress	199.9 ± 8.69	Veh without stress – Veh with stress	***	14
Glut + L-serine	154.5 ± 14.16	Veh with stress – Glut + L-serine	*	8
Glut	143.3 ± 14.85	Veh with stress – Glut	*	6
L-serine	195.3 ± 19.43	Veh without stress – L-serine	*	4
TST in non-stressed rats with chronic microinfusion of NMDA (**Figure 1E**)				
Treatment	Immobility (s)	Comparison (One way ANOVA) ("– "compared groups)	Significance	n
Veh without stress	134.4 ± 7.32			17
NMDA	213.5 ± 32.32	Veh without stress – NMDA	**	4
TST in rats with chronic restraint stress and chronic microinfusion tested on day 18 (**Figure 1F**)				
Treatment	Immobility (s)	Comparison (One way ANOVA) ("– " compared groups)	Significance	n
Veh with stress	214.0 ± 8.216			4
TAT-L2	98.80 ± 11.62	Veh with stress – TAT-L2	***	5
TAT-L2 + Glut + D-serine	192.7 ± 14.19	TAT-L2 – TAT-L2 + Glut+ D-serine	***	3
Figure 2. Acute Cx43 hemichannel blockade with TAT-L2 into the ventral hippocampus induces antidepressant effects after chronic restraint stress, which can be prevented by D-serine and glutamate				
TST in rats with or without chronic restraint stress with acute microinjection of TAT-L2, glutamate and D-serine (**Figure 2B**)				

Treatment	Immobility (s)	Comparison (One way ANOVA) ("– "compared groups)	Significance	n
Veh without stress	117.7 ± 10.12			6
Veh with stress	211.4 ± 12.78	veh without stress – veh with stress	***	14
Glut + D-serine	225.0 ± 11.17	Veh without stress - Glut + D-serine-TAT-L2 - Glut + D-serine	***	4
TAT-L2	119.4 ± 10.73	Veh with stress – TAT -TAT + Glut + D-serine	*** *	8
TAT -L2 + Glut + D-serine	207.3 ± 10.33	Veh without stress – TAT + Glut + D-serine	*	3
TST in rats with or without chronic restraint stress, with acute microinjection of TAT-L2, glutamate and L-serine (**Figure 2C**)				
Treatment	Immobility (s)	Comparison (One way ANOVA) ("– " compared groups)	Significance	n
Veh without stress	117.7 ± 10.12			6
Veh with stress	217.3 ± 13.24	Veh without stress – Veh with stress	***	15
TAT-L2	128.0 ± 10.82	Veh with stress – TAT-L2	***	8
TAT-L2 + Glut + L-Serine	194.4 ± 7.71	Veh without stress -TAT-L2 + Glut + L-Serine TAT-L2 -TAT-L2 + Glut + L-Serine	** *	7
FST in rats with chronic restraint stress and acute microinjection of TAT-L2, glutamate and D-serine (**Figure 2D**)				
Treatment	Immobility (s)	Comparison (One way ANOVA) ("– " compared groups)	Significance	n
Veh with stress	148.3 ± 13.65			18
TAT-L2	57 ± 11.32	Veh with stress – TAT-L2	***	12
TAT-L2 + Glut + D-serine	134.4 ± 7.65	TAT-L2 – TAT-L2 + Glut + D-serine	**	7
FST after chronic restraint stress and acute microinjection of TAT-L2, glutamate and L-serine (**Figure 2E**)				
Treatment	Immobility (s)	Comparison (One way ANOVA) ("– "compared groups)	Significance	n
Veh with stress	148.3 ± 13.65			18
TAT-L2	57 ± 11.32	Veh with stress – TAT-L2	***	12
TAT-L2 + Glut + L-serine	173.4 ± 7.84	TAT-L2 – TAT-L2 + Glut + L-serine	***	5
TST in rats with chronic unpredictable mild stress and acute microinjection of TAT-L2, glutamate and D-serine **(Figure 2F)**				
Treatment	Immobility (s)	Comparison (One way ANOVA) ("– "compared groups)	Significance	n
Veh without stress	117.7 ± 10.12			6
Veh with stress	196.7 ± 6.55	Veh without stress - Veh with stress	***	6
TAT-L2	143.5 ± 8.02	Veh with stress - TAT-L2	***	6
TAT-L2 + Glut + D-serine	212.4 ± 6.59	TAT-L2 - TAT-L2 + Glut + D-serine Veh without stress - TAT-L2 + Glut + D-serine	*** ***	7
% Etd^+ uptake in hippocampal slices post chronic restraint stress **(Figure 2H)**				
Treatment	% Etd^+ uptake	Comparison (One way ANOVA) ("– " compared groups)	Significance	n
Veh without stress	100 ± 0			3
Veh with stress	188.8 ± 2.84	Veh without stress – Veh with stress	***	3
TAT-L2 + stress	63.99 ± 1.81	Veh without stress – TAT-L2 with stress	** ***	3

		Veh with stress – TAT-L2 with stress		
TAT-L2	51.09 ± 9.86	Veh without stress – TAT-L2 without stress Veh with stress – TAT-L2 without stress	*** ***	3
Extracellular glutamate from hippocampal slices post chronic stress (**Figure 2I**)				
Treatment	Glutamate (nmol/ml)	Comparison (One way ANOVA) ("– "compared groups)	Significance	n
Veh without stress	95.57 ± 2.797			3
Veh with stress	148.6 ± 2.108	Veh without stress – Veh with stress	***	3
TAT-L2 + stress	99.90 ± 4.396	Veh with stress – TAT-L2 with stress	***	3
TAT-L2	94.84 ± 5.685	Veh with stress – TAT-L2 without stress	***	3
Figure 3. TAT-L2 on hippocampal postsynaptic NMDAR activity fEPSPs in hippocampal slices **(Figure 3A)**				
Treatment	Response amplitude (%basal)	Comparison (Kruskal-Wallis test) ("-"comparated groups)	Significance	n
Basal	100.2 ± 0.18			6
TAT-L2	76.03 ± 3.68	Basal – TAT-L2	*	6
TAT-L2 + Glut + D-serine	94.99 ± 9.35			6
Figure 4. Cacotheline on Cx43 hemichannel activity in transfected HeLa and DITNC 1 astroglial cell line				
DAPI uptake in HeLa cells transfected with Cx30 and Cx43 under normal Ca^{2+} conditions and 0.1μM cacotheline **(Figure 4B)**				
Treatment	Average (%) labeled/total cells	Comparison (ANOVA) ("– " compared groups)	Significance	n
WT	2.597 ± 0.44			3
Cx30	4.033 ± 1.27			3
Cx43	3.840 ± 1.096			3
DAPI uptake in HeLa cells transfected with Cx30 and Cx43 in response to 0.1μM of cacotheline under Ca^{2+} free conditions **(Figure 4C)**				
Treatment	Average (%) labeled/total cells	Comparison (ANOVA) ("– " compared groups)	Significance	n
WT	2.310 ± 0.57			3
Cx30	87.55 ± 4.78	WT – Cx30	***	3
Cx43	1.220 ± 0.62	Cx30- Cx43	***	3
DAPI uptake in DI TNC1 astrocytes in response to 0.1μM of cacotheline under normal Ca^{2+} conditions **(Figure 4E)**				
Treatment	Average (%) labeled/total cells	Comparison (ANOVA) ("– " compared groups)	Significance	n
Control	9.096 ± 0.42			3
TAT-L2	6.944 ± 0.92			3
Cacotheline	10.02 ± 0.87			3
DAPI uptake in DI TNC1 astrocytes in response to 0.1μM of cacotheline under Ca^{2+} free conditions **(Figure 4F)**				
Treatment	Average (%) labeled/total cells	Comparison (ANOVA) ("– " compared groups)	Significance	n
Control	89.89 ± 1.38			3
TAT-L2	7.689 ± 0.28	Control – TAT-L2	***	3

Cacotheline	10.87 ± 0.46	Control – Cacotheline	***	3
Figure 5. Cacotheline reductions of hippocampal postsynaptic NMDAR activity and its antidepressant effects when injected intraperitoneally.				
Effects of cacotheline on postsynaptic NMDAR activity (fEPSP) slope of input/output curves **(Figure 5A)**				
Treatment	Slope of input/output curves	Comparison (one-way ANOVA) ("– " compared groups)	Significance	n
Control	0.01563 ± 0.000096			3
Cacotheline	0.005220 ± 0.001619	Control – Cacotheline	***	3
Cacotheline + D-serine	0.008822 ± 0.0003697	Control – Cacotheline + D-serine Cacotheline – Cacotheline + D-serine	*** *	3
Cacotheline + Glutamate	0.009477 ± 0.0001854	Control – Cacotheline + Glutamate Cacotheline – Cacotheline + Glutamate	** *	3
Cacotheline + D-serine + Glutamate	0.009944 ± 0.0003599	Control – Cacotheline + D-serine + Glutamate Cacotheline – Cacotheline + D-serine +Glutamate	** **	3
TST in rats with chronic restraint stress, injected with cacotheline i.p. post stress **(Figure 5B)**				
Treatment	Immobility (s)	Comparison (Mann Whitney) ("– " compared groups)	Significance	n
Veh	54.50 ± 3.74			8
Cacotheline	23.13 ± 10.70	Veh – Caco	*	8
FST in rats with chronic restraint stress, injected with cacotheline post stress **(Figure 5C)**				
Treatment	Immobility (s)	Comparison (unpaired t test) ("– " compared groups)	Significance	n
Veh	166.3 ± 8.35			15
Cacotheline	133.1 ± 10.22	Veh- Caco	*	15
TST in rats with chronic restraint stress injected with Ketamine post stress **(Figure 5D)**				
Treatment	Immobility (s)	Comparison (ANOVA) ("– " compared groups)	Significance	n
Veh	158.7 ± 16.51			12
Ket	100.5 ± 22.41	Veh – Ket	*	8
TST in rats with chronic stress administered with oral fluoxetine **(Figure 5E)**				
Treatment	Immobility (s)	Comparison (unpaired t test) ("– " compared groups)	Significance	n
Veh	160.6 ± 8.05			22
Flx	120.9 ± 16.78	Veh – Flx	*	7
Transitions in the openfield after cacotheline i.p administration **(Figure 5F)**				
Treatment	Immobility (s)	Comparison (unpaired t test) ("– " compared groups)	Significance	n
Veh	52.17 ± 8.16			6
Cacotheline	77.6 ± 15.65			5
% Etd^+ uptake in astrocytes from hippocampal slices after post-stress cacotheline i.p. administration **(Figure 5H)**				
Treatment	Average (%) labeled/total cells	Comparison (one way ANOVA) ("– " compared groups)	Significance	n
Veh without stress	100 ± 0	Veh without stress – Veh with stress	***	3
Veh with stress	175.5 ± 2.95		***	3

Cacotheline	82.16 ± 6.16	Veh with stress – Caco	***	3
TAT-L2 + stress	69.05 ± 5.08	Veh without stress – TAT-L2 + stress Veh with stress – TAT-L2 + stress	* ***	3
TAT-L2	60.41 ± 11.38	Veh without stress – TAT-L2 Veh with stress – TAT-L2	** ***	3
Extracellular glutamate from hippocampal slices with or without post-stress cacotheline i.p. administration **(Figure 5l)**				
Treatment	Glutamate (nmol/ml)	Comparison (one wayANOVA) ("– " compared groups)	Significance	n
Veh without stress	109.6 ± 1.03			4
Veh with stress	149.1 ± 4.81	Veh without stress – Veh with stress	***	4
Cacotheline	113.5 ± 3.42	Veh with stress – Caco	***	4
TAT-L2 + stress	105.2 ± 4.51	Veh with stress – TAT-L2 + stress	***	4
TAT-L2	111.3 ± 2.63	Veh with stress – TAT-L2	***	4
Figure S1. Controls for *in vivo* experiments.				
TST in rats with or without chronic restraint stress, with chronic intra-hippocampal microinfusions **(Figure S1A)**				
Treatment	Immobility (s)	Comparison (one way ANOVA) ("– " compared groups)	Significance	n
Veh without stress	129.4 ± 8.35			12
Veh with stress	199.9 ± 8.69	Veh without stress –Veh with stress	***	14
TAT-L2	94.60 ± 13.99	Veh with stress – TAT-L2	***	5
TAT-L2 + Glut	117 ± 8.14	Veh with stress – TAT-L2 + Glut	***	5
TAT-L2 + D-serine	102.8 ± 9.67	Veh with stress – TAT-L2 + D-serine	***	5
TST in rats with or without chronic stress with acute post-stress intra-hippocampal microinjections **(Figure S1B)**				
Treatment	The time spent struggling (s)	Comparison (one way ANOVA) ("– " compared groups)	Significance	n
Veh without stress	203.8 ± 16.31			6
Veh with stress	147.5 ± 12.29	Veh without stress - Veh with stress	*	12
TAT-L2	233.8 ± 12.20	Veh with stress - TAT-L2	***	8
TAT-L2 + Glut +´D-serine	132.7 ± 16.34	TAT-L2 - TAT-L2 + Glut + D-serine	**	3
TST in rats with or without chronic stress with acute post-stress intra-hippocampal microinjections **(Figure S1C)**				
Treatment	Immobility (s)	Comparison (one way ANOVA) ("– " compared groups)	Significance	n
Veh	117.7 ± 10.12			6
Veh	217.3 ± 13.24	Veh without stress – Veh with stress	***	15
TAT-L2	128.0 ± 10.82	Veh with stress – TAT-L2	***	8
TAT-L2 + Glut	130.0 ± 12.01	Veh with stress – TAT-L2 + Glut	*	3
TAT-L2 + D-serine	118.8 ± 18.05	Veh with stress – TAT-L2 + D-serine	***	5
TAT-L2 + L-serine	118.3 ± 16.46	Veh with stress – TAT-L2 + L-serine	**	3
TST in rats with or without chronic restraint stress with acute post-stress intra-hippocampal microinjections **(Figure S1D)**				
Treatment	Immobility (s)	Comparison (one way ANOVA) ("– " compared groups)	Significance	n
Veh without stress	117.7 ± 10.12			6
Veh with stress	211.4 ± 12.78	Veh without stress - Veh with stress	***	14

TAT-L2	137.3 ± 9.21	Veh with stress – TAT-L2	*	4
FST in rats with or without chronic restraint stress with acute post-stress intra-hippocampal microinjections **(Figure S1E)**				
Treatment	Immobility (s)	Comparison (one way ANOVA) ("– " compared groups)	Significance	n
Veh with stress	148.3 ± 13.65			18
TAT-L2	58.6 ± 10.14	Veh with stress – TAT-L2	***	15
TAT-L2 + Glut	99 ± 17.16			10
TAT-L2 + D-serine	148.6 ± 5.653	TAT-L2 - TAT-L2 + D-serine	**	5
TAT-L2 + L-serine	165.3 ± 19.77	TAT-L2 - TAT-L2 + L-serine	**	3
Percentage of GFAP+ astrocytes with Etd+ uptake in hippocampal slices **(Figure S1F)**				
Treatment	% of cells	Comparison (one way ANOVA) ("– " compared groups)	Significance	n
Veh without stress	11.93 ± 0-9939			
Veh with stress	31.00 ± 2.082	Veh with stress – Veh without stress	***	3
TAT-L2 with stress	10.00 ± 0.5774	Veh with stress – TAT-L2 with stress	***	3
TAT-L2 without stress	7.68 ± 0.3333	Veh with stress – TAT-L2 without stress	***	3
Percentage of non-GFAP cells with Etd+ uptake in hippocampal slices **(Figure S1G)**				
Treatment	% of cells	Comparison (one way ANOVA) ("– " compared groups)	Significance	n
Veh without stress	17.00 ± 1.528			
Veh with stress	36.00 ± 2.309	Veh with stress – Veh without stress	***	3
TAT-L2 with stress	31.33 ± 1.856	Veh with stress – TAT-L2 with stress		3
TAT-L2 without stress	18.00 ± 0.5774	Veh with stress – TAT-L2 without stress	***	3
APV on hippocampal postsynaptic NMDAR activity fEPSPs in ventral hippocampal slices **(Figure S2B)**				
Treatment	Response amplitude (%basal)	Comparison (Kruskal-Wallis test) ("-"comparated groups)	Significance	n
Basal	100.2 ± 0.1843			6
TAT-L2 +Glut	95.18 ± 3.514			3
TAT-L2 + D-serine	92.37 ± 16.66	APV – TAT-L2 + D-serine	*	3
APV	34.27 ± 2.027	Basal – APV	**	6
Figure S3: Cx43 and Cx30 hemichannel activity in HeLa, Cx43 hemichannel activity in DIT NC1 astrocytes				
DAPI uptake in HeLa expressing Cx30 and 43 exposed to 1µM of cacotheline under normal Ca^{2+} conditions. **(Figure S3A)**				
Treatment	Average (%) labeled/total cells	Comparison ((Kruskal-Wallis test) ("– " compared groups)	Significance	n
WT	4.027 ± 1.767			3
Cx30	3.513 ± 0.4034			3
Cx43	4.243 ± 1.069			3
DAPI uptake in HeLa expressing Cx30 and 43 exposed to 1µM of cacotheline under Ca^{2+} free conditions. **(Figure S3B)**				
Treatment	Average (%) labeled/total cells	Comparison (one way ANOVA) ("– " compared groups)	Significance	n
WT	4.883 ± 0.8761			3

Cx30	91.52 ± 3.528	WT – Cx30	***	3
Cx43	2.287 ± 0.7672	Cx30 – Cx43	***	3
DAPI uptake in DI TNC1 astrocytes in response to 1μM cacotheline under normal Ca^{2+} conditions **(Figure S3C)**				
Treatment	Average (%) labeled/total cells	Comparison (one way ANOVA) ("– " compared groups)	Significance	n
Control	9.096 ± 0.4233			3
TAT-L2	6.944 ± 0.9171			3
Cacotheline	9.490 ± 0.6430			3
DAPI uptake in DI TNC1 astrocytes in response to 1μM cacotheline under Ca^{2+} free conditions **(Figure S3D)**				
Treatment	Average (%) labeled/total cells	Comparison (one way ANOVA) ("– " compared groups)	Significance	n
Control	89.89 ± 1.383			3
TAT-L2	7.689 ± 0.2804	Control – TAT-L2	***	3
Cacotheline	9.540 ± 0.5575	Control – Cacotheline	***	3
Figure S4. Effect of TAT-Cx43 L2 and cacotheline on astroglial Cx43 gap junctional coupling in primary astroglial culture and on postsynaptic NMDAR activity in the dorsal hippocampus				
Slope of input/output curves in hipocampal slices **(Figure S4B)**				
Treatment	Average (%) labeled/total cells	Comparison (one way ANOVA)("– " compared groups)	Significance	n
Vehicle	0.01560 ± 0.00009			5
TAT-L2	0.01037 ± 0.001001	Control – TAT-L2	***	3
TAT-L2 + D-serine	0.01512 ± 0.00067	TAT-L2 – TAT-L2 + D-serine Cacotheline – Cacotheline + D-serine	*** *	3
TAT-L2 + glutamate	0.01441 ± 0.00056	TAT-L2 – TAT-L2 + Glutamate	***	3
TAT-L2 + glutamate + D-serine	0.01693 ± 0.00018	TAT-L2 – TAT-L2 + D-serine +Glutamate TAT-L2 + Glutamate + TAT-L2 + D-serine +Glutamate	*	5
Figure S5. Effect of cacotheline on astroglial Cx43 gap junctional coupling and its effect on organ function				
TST in rats with chronic restraint stress and acute microinfusion of cacotheline on day 11 and tested on day 18 **(Figure S5A)**				
Treatment	Immobility (s)	Comparison (one way ANOVA) ("– " compared groups)	Significance	n
Veh without stress	124.0 ± 12.36			10
Veh with stress	176.0 ± 8.361	Veh without stress - Veh with stress	*	5
Cacotheline	192.2 ± 12.89	Veh with stress - Cacotheline	**	6

Supplementary Table 1. Results data and statistics. All results are shown in the table, ordered by Figure, with the treatment, value, interactions showing significant differences, type of statistical test and level of significance *p<0.05, **p<0.01, ***p<0.001. In all cases normality was tested and appropriate tests were used. When using ANOVA, it was followed by the Tukey *post hoc* test. Vehicle (Veh); TAT-Cx43L2 (TAT-L2); cacotheline (Caco); glutamate (Glut).

Complementary Discussion

It is important to note that rodent depressive-like behaviors such as learned helplessness, anhedonia, and decreased social interactions are used as surrogates for human depressive symptoms but do not capture the full spectrum of human depressive experiences. Further studies are needed to advance our understanding of the role of astroglial gliotransmitter release in depression-associated behaviors such as memory deficits and sleep disturbances.

There is ample evidence that the antidepressant effects of ketamine are mediated by its NMDAR antagonism (5). While other NMDAR antagonists show antidepressant effects in animal models of depression (6), only ketamine has antidepressant effects in depressed patients (reviewed in (7)). It has been proposed that ketamine show may be different to other NMDAR antagonists due to its preferential inhibition of NMDARs localized in inhibitory interneurons, its activity-dependent NMDAR antagonism and possible differences in its effects on tonically activated specific NMDAR subunits (reviewed in (7)). Studies have also shown that besides NMDAR antagonism, ketamine increases postsynaptic mTOR, p70S6K, and 4E-BP1, BDNF transcription and inhibition of GSK-3, among others (reviewed in (8)). Further research is required to determine the extent to which the antidepressant effects induced by astroglial Cx43 hemichannel blockade affect the intracellular pathways activated by ketamine. Previous studies have shown that acute intra-hippocampal microinjection of NMDA can induce depressive-like symptoms, while the intra-hippocampal microinfusion of NMDAR antagonist MK801 can prevent the development of chronic stress-induced depressive-like symptoms (9–11). Consequently, it is likely that the decrease of postsynaptic NMDAR activity obtained either directly via ketamine and/or through astroglial Cx43 hemichannel blockade, could lead to similar antidepressant effects.

Previous studies have suggested that chronic restraint stress induces a decrease in the number and density of GFAP+ cells (12–14) and a reduction in astroglial cell volume, arbor area and lacunarity in the ventral hippocampus and dentate gyrus (13, 14), changes that were counteracted by fluoxetine treatment (15). Future studies should determine whether continuous TAT-L2 intra-hippocampal microinfusion during chronic stress can prevent the morphological changes in astrocytes induced by chronic stress.

In the experiments utilizing chronic release through osmotic pumps, TAT-L2 was continuously administered for 14 days. Given that it prevented the development of depressive symptoms, as evidenced by the absence of symptoms in rats on day 18, it is likely that TAT-L2 remained biologically active throughout the entire 14-day period. However, considering that TAT-L2 is a peptide, it is possible that it degraded overtime, so the possibility that its effects took place during the first days of stress cannot be ruled out.

Similar to the effects observed in the BLA during cued fear memory training (16, 17), under non-stressed conditions, blocking Cx43 hemichannel activity in the hippocampus would most likely impair both NMDAR-dependent synaptic plasticity and reference spatial memory. However, chronic stress induces an

increase in post synaptic NMDAR activity in the hippocampus (18, 19) and impairs NMDAR-mediated synaptic plasticity in the hippocampus (20–23), due to the excess of NMDAR activity through an inverted U effect, changes in the expression of AMPAR and NMDAR subunits (24–27), and other factors (reviewed in (21), which may contribute to stress-associated spatial memory deficits (28, 29). Therefore, short-term Cx43 hemichannel blockade in chronic stress-induced depression could reduce NMDAR activity sufficiently to reactivate NMDAR-dependent synaptic plasticity and in the long-term, contribute to decreasing glutamate, ATP and D-serine build up, possibly restoring hippocampal synaptic plasticity and spatial memory. Further experiments should be performed to assess this possibility.

Our previous research (16, 17) showed that in cued fear conditioning, blocking Cx43 hemichannel activity in the BLA impeded short-term memory and memory consolidation. This effect was prevented by the addition of a mixture of glutamate and D-serine, but not by either compound alone or by a combination of glutamate and glycine, suggesting a role for synaptic NMDARs rather than extrasynaptic NMDARs, as glycine acts as a co-agonist on extrasynaptic GluN2B-containing NMDARs, whereas D-serine acts on synaptic GluN2A-containing NMDARs (30). Although we did not test the ability of a combination of glutamate and glycine to reverse the decrease in NMDAR activity induced by TAT-Cx43L2 in the present report, the reversion by glutamate and D-serine strongly suggests a role for synaptic NMDARs, likely involving GluN2A-containing NMDARs.

A study by Portal and colleagues reported that the intra-hippocampal reduction of Cx43 via the injection of a shRNA against Cx43 or the acute systemic injection of a non-selective Cx inhibitor increased the antidepressant effects of fluoxetine (31). Therefore, it is likely that the blockade of Cx43 hemichannels via cacotheline or D4 may increase the efficacy for antidepressants such as fluoxetine. This could be especially relevant for patients that show only partial improvements with current antidepressants.

Astroglial Cx43 hemichannels have been shown to regulate postsynaptic NMDAR activity in the prefrontal cortex (PFC) via D-serine (24). Therefore, blocking Cx43 hemichannels in this region could potentially yield antidepressant effects. This aligns with findings that peripheral administration of cacotheline, which likely penetrated the entire brain, had antidepressant effects. However, it is important to recognize that the effects of chronic stress may differ between the hippocampus and the PFC. Therefore, future research should investigate the effects of Cx43 hemichannel blockade in the PFC within the context of depression.

The acute administration of cacotheline did not result in any noticeable behavioral deficits or sedation, as evaluated in the openfield test, nor did it impact markers of organ function. Additionally, chronic administration of cacotheline at its effective dose did not cause lethality, thereby ruling out cardiotoxicity, which would typically manifest as behavioral deficits and lethality. However, Cx43 gap junctions are essential for calcium propagation during heartbeats, enabling synchronized myocardial contraction. Therefore, the safety profile of any future drug targeting Cx43 hemichannels must rigorously exclude cardiac toxicity due to unintended effects on Cx43 gap junctions. Previous studies in rodents have shown that blocking Cx43 hemichannels with peptides that interact with the Cx43 C-terminal (such as TAT-

Cx43L2, GAP19, or αCT1) did not adversely affect overall cardiac function (32), even demonstrated cardioprotective effects in several models of cardiac dysfunction. These include protection against isoproterenol-induced arrhythmia in a rodent model of muscular dystrophy (33) and against cardiac ischemia-reperfusion injury (32, 34). However, further research is necessary to examine both the potential short- and long-term effects of chronic administration of Cx43 hemichannel blockers like cacotheline or D4 on both gross and more detailed cardiac function, such as sinus rhythm, sino-atrial, atrio-ventricular and intraventricular conduction.

References

1. H. Li, *et al.*, Rifaximin-mediated gut microbiota regulation modulates the function of microglia and protects against CUMS-induced depression-like behaviors in adolescent rat. *J Neuroinflammation* **18**, 254 (2021).

2. I. E. Alfaro, L. Varela-Nallar, M. Varas-Godoy, N. C. Inestrosa, The ROR2 tyrosine kinase receptor regulates dendritic spine morphogenesis in hippocampal neurons. *Molecular and Cellular Neuroscience* **67**, 22–30 (2015).

3. S. Kaech, G. Banker, Culturing hippocampal neurons. *Nat Protoc* **1**, 2406–2415 (2006).

4. P. Lipp, E. Niggli, Ratiometric confocal Ca2+-measurements with visible wavelength indicators in isolated cardiac myocytes. *Cell Calcium* **14**, 359–372 (1993).

5. P. Zanos, *et al.*, NMDA RECEPTOR ACTIVATION-DEPENDENT ANTIDEPRESSANT-RELEVANT BEHAVIORAL AND SYNAPTIC ACTIONS OF KETAMINE. *J. Neurosci.* JN-RM-1316-22 (2023). https://doi.org/10.1523/JNEUROSCI.1316-22.2022.

6. R. Trullas, P. Skolnick, Functional antagonists at the NMDA receptor complex exhibit antidepressant actions. *European Journal of Pharmacology* **185**, 1–10 (1990).

7. T. D. Gould, C. A. Zarate, S. M. Thompson, Molecular Pharmacology and Neurobiology of Rapid-Acting Antidepressants. *Annu. Rev. Pharmacol. Toxicol.* **59**, 213–236 (2019).

8. J. W. Murrough, C. G. Abdallah, S. J. Mathew, Targeting glutamate signalling in depression: progress and prospects. *Nat Rev Drug Discov* **16**, 472–486 (2017).

9. A. S.-C. [DONG Su-Ping XU Chang, YUAN Ting-Ting, Hippocampal NMDA Receptor is involved in Chronic Stress Induced Depressive-Like Behaviors via SP-NK1 Receptor Pathway. *Acta Psychologica Sinica* **43**, 1045–1054 (2011).

10. Y. Ling, S.-C. An, T. Lian, Involvement of hippocampal NMDA receptor and neuropeptide Y in depression induced by chronic unpredictable mild stress. *Sheng Li Xue Bao* **62**, 14–22 (Feb 25).

11. H. Liu, L.-M. Wen, H. Qiao, S.-C. An, Modulation of hippocampal glutamate and NMDA/AMPA receptor by homocysteine in chronic unpredictable mild stress-induced rat depression. *Acta Physiologica Sinica* **65**, 61–71 (Feb 25).

12. M. A. Orlovsky, V. E. Dosenko, F. Spiga, G. G. Skibo, S. L. Lightman, Hippocampus remodeling by chronic stress accompanied by GR, proteasome and caspase-3 overexpression. *Brain Research* **1593**, 83–94 (2014).

13. P. Sántha, *et al.*, Restraint Stress-Induced Morphological Changes at the Blood-Brain Barrier in Adult Rats. *Front. Mol. Neurosci.* **8** (2016).

14. N. Perez-Urrutia, *et al.*, Intranasal cotinine improves memory, and reduces depressive-like behavior, and GFAP + cells loss induced by restraint stress in mice. *Experimental Neurology* **295**, 211–221 (2017).

15. B. Czéh, *et al.*, Chronic Social Stress Inhibits Cell Proliferation in the Adult Medial Prefrontal Cortex: Hemispheric Asymmetry and Reversal by Fluoxetine Treatment. *Neuropsychopharmacol* **32**, 1490–1503 (2007).

16. J. Stehberg, *et al.*, Release of gliotransmitters through astroglial connexin 43 hemichannels is necessary for fear memory consolidation in the basolateral amygdala. *FASEB j.* **26**, 3649–3657 (2012).

17. S. Linsambarth, *et al.*, Astroglial gliotransmitters released via Cx43 hemichannels regulate NMDAR-dependent transmission and short-term fear memory in the basolateral amygdala. *The FASEB Journal* **36** (2022).

18. M. Popoli, Z. Yan, B. S. McEwen, G. Sanacora, The stressed synapse: the impact of stress and glucocorticoids on glutamate transmission. *Nat Rev Neurosci* **13**, 22–37 (2011).

19. W. N. Marsden, Stressor-induced NMDAR dysfunction as a unifying hypothesis for the aetiology, pathogenesis and comorbidity of clinical depression. *Medical Hypotheses* **77**, 508–528 (2011).

20. C. Pavlides, L. G. Nivón, B. S. McEwen, Effects of chronic stress on hippocampal long-term potentiation. *Hippocampus* **12**, 245–257 (2002).

21. W. N. Marsden, Synaptic plasticity in depression: Molecular, cellular and functional correlates. *Progress in Neuro-Psychopharmacology and Biological Psychiatry* **43**, 168–184 (2013).

22. M. Gross, *et al.*, Early onset of cognitive impairment is associated with altered synaptic plasticity and enhanced hippocampal GluA1 expression in a mouse model of depression. *Neurobiology of Aging* **36**, 1938–1952 (2015).

23. X. Shang, Y. Shang, J. Fu, T. Zhang, Nicotine Significantly Improves Chronic Stress-Induced Impairments of Cognition and Synaptic Plasticity in Mice. *Mol Neurobiol* **54**, 4644–4658 (2017).

24. N. Yilmaz, *et al.*, Effects of Venlafaxine and Escitalopram Treatments on NMDA Receptors in the Rat Depression Model. *J Membrane Biol* **242**, 145–151 (2011).

25. V. Duric, *et al.*, Altered expression of synapse and glutamate related genes in post-mortem hippocampus of depressed subjects. *International Journal of Neuropsychopharmacology* **16**, 69–82 (2013).

26. M. Sowa-Kućma, *et al.*, Zinc, magnesium and NMDA receptor alterations in the hippocampus of suicide victims. *Journal of Affective Disorders* **151**, 924–931 (2013).

27. L. Zhang, *et al.*, RAGE signaling pathway is involved in CUS-induced depression-like behaviors by regulating the expression of NR2A and NR2B in rat hippocampus DG. *Experimental Neurology* **361**, 114299 (2023).

28. A. N. Hoffman, *et al.*, Recovery after chronic stress within spatial reference and working memory domains: correspondence with hippocampal morphology. *Eur J of Neuroscience* **34**, 1023–1030 (2011).

29. C. D. Conrad, A critical review of chronic stress effects on spatial learning and memory. *Progress in Neuro-Psychopharmacology and Biological Psychiatry* **34**, 742–755 (2010).

30. T. Papouin, *et al.*, Synaptic and Extrasynaptic NMDA Receptors Are Gated by Different Endogenous Coagonists. *Cell* **150**, 633–646 (2012).

31. B. Portal, *et al.*, Genetic and pharmacological inactivation of astroglial connexin 43 differentially influences the acute response of antidepressant and anxiolytic drugs. *Acta Physiol* **229** (2020).

32. J. Jiang, *et al.*, Interaction of α Carboxyl Terminus 1 Peptide With the Connexin 43 Carboxyl Terminus Preserves Left Ventricular Function After Ischemia-Reperfusion Injury. *JAHA* **8**, e012385 (2019).

33. J. P. Gonzalez, J. Ramachandran, L.-H. Xie, J. E. Contreras, D. Fraidenraich, Selective Connexin43 Inhibition Prevents Isoproterenol-Induced Arrhythmias and Lethality in Muscular Dystrophy Mice. *Sci Rep* **5**, 13490 (2015).

34. N. Wang, *et al.*, Selective inhibition of Cx43 hemichannels by Gap19 and its impact on myocardial ischemia/reperfusion injury. *Basic Res Cardiol* **108**, 309 (2013).